

1 **Impact of Athabasca oil sands operations on mercury levels in air and deposition**

2

3 Ashu Dastoor<sup>1</sup>, Andrei Ryjkov<sup>1</sup>, Gregor Kos<sup>2</sup>, Junhua Zhang<sup>3</sup>, Jane Kirk<sup>4</sup>, Matthew Parsons<sup>5</sup> and  
4 Alexandra Steffen<sup>3</sup>

5 <sup>1</sup>Air Quality Research Division, Environment and Climate Change Canada, 2121 Trans-Canada  
6 Highway, Dorval, Québec, Canada

7 <sup>2</sup>Department of Chemistry and Biochemistry, Concordia University, 7141 Sherbrooke Street  
8 West, Montreal, Québec, Canada

9 <sup>3</sup>Air Quality Research Division, Environment and Climate Change Canada, 4905 Dufferin Street,  
10 Toronto, Ontario, Canada

11 <sup>4</sup>Aquatic Contaminants Research Division, Environment and Climate Change Canada, 867  
12 Lakeshore Road, Burlington, Ontario, Canada

13 <sup>5</sup> Meteorological Service of Canada, Environment and Climate Change Canada, 9250 49 Street  
14 NW, Edmonton, Alberta, Canada

15

16 **Correspondence:** Ashu Dastoor (ashu.dastoor@canada.ca)

17

18 **Abstract**

19 Oil sands upgrading facilities in the Athabasca Oil Sands Region (AOSR) in Alberta, Canada, have  
20 been reporting mercury (Hg) emissions to public government databases (National Pollutant  
21 Release Inventory (NPRI)) since the year 2000, yet the relative contribution of these emissions to  
22 ambient Hg deposition remains unknown. The impact of oil sands emissions (OSE) on Hg levels  
23 in and around the AOSR, relative to contributions from global (anthropogenic, geogenic and  
24 legacy) emissions and regional biomass burning emissions (BBE), was assessed using a 3D  
25 process-based global Hg model, GEM-MACH-Hg, from 2012 to 2015. In addition, the relative  
26 importance of year-to-year changes in Hg emissions from the above sources and meteorological  
27 conditions to inter-annual variations in Hg deposition was examined. Surface air concentrations of  
28 Hg species and annual snowpack Hg loadings simulated by the model were found comparable to  
29 measured levels in the AOSR, suggesting consistency between reported Hg emissions from oil  
30 sands activities and Hg levels in the region. As a result of global-scale transport and long lifetime  
31 of gaseous elemental Hg (Hg(0)), surface air concentrations of Hg(0) in the AOSR reflected the

32 background Hg(0) levels in Canada. By comparison, average air concentrations of total oxidised  
33 Hg (efficiently deposited Hg species) in the AOSR were elevated up to 60% within 50 km of the  
34 oil sands Hg emission sources. Hg emissions from wildfire events led to episodes of high ambient  
35 Hg(0) concentrations and deposition enrichments in northern Alberta, including the AOSR, during  
36 the burning season. Hg deposition fluxes in the AOSR were within the range of the deposition  
37 fluxes measured for the entire province of Alberta. On a broad spatial scale, contribution from  
38 imported Hg from global sources dominated the annual background Hg deposition in the AOSR,  
39 with present-day global anthropogenic emissions contributing to 40% (< 1% from Canada  
40 excluding OSE), and geogenic and legacy emissions contributing to 60% of the background Hg  
41 deposition. In contrast, oil sands Hg emissions were responsible for significant enhancements in  
42 Hg deposition in the immediate vicinity of oil sands Hg emission sources, which were ~10 times  
43 larger in winter than summer (250 – 350% in winter and ~35% in summer within 10 km of OSE,  
44 2012-2013). The spatial extent of the influence of oil sands emissions on Hg deposition was also  
45 greater in winter relative to summer (~100 km vs 30 km from Hg emitting facilities). In addition,  
46 inter-annual changes in meteorological conditions and oil sands emissions also led to significantly  
47 higher inter-annual variations in wintertime Hg deposition compared to summer. For example, a  
48 large snowmelt event at the end of February in 2015 effectively removed about half of the  
49 accumulated mercury in snow, contributing to (observed and modeled) low annual snow Hg  
50 loadings. Inter-annual variations in meteorological conditions were found to both exacerbate and  
51 diminish the impacts of OSE on Hg deposition in the AOSR, which can confound the interpretation  
52 of trends in short-term environmental Hg monitoring data. In winter, within 10 km of major oil  
53 sands sources, variations in meteorology led to Hg deposition reduction by 17% in 2014 and  
54 increase by 10% in 2015 and decline in OSE lowered Hg deposition by 35% (2014) and 56% (  
55 2015), resulting in overall reductions in wintertime Hg deposition of 52% (2014) and 46% (2015),  
56 relative to 2012. By comparison, annually, changes in meteorology and BBE in 2014-2015  
57 (relative to 2012) led to Hg deposition increases of 1-6% and 2%, respectively, and decline in OSE  
58 lowered deposition by 15-22%, resulting in overall reduction in Hg deposition of 7-20% within 10  
59 km of oil sands sources. Hg runoff in spring flood, comprising the majority of annual Hg runoff,  
60 is mainly derived from seasonal snowpack Hg loadings and mobilization of Hg deposited in  
61 surface soils, both of which are sensitive to Hg emissions from oil sands developments in  
62 proximity of sources. Model results suggest that sustained efforts to reduce anthropogenic Hg

63 emissions from both global and oil sands sources are required to reduce Hg deposition in the  
64 AOSR.

65

## 66 **Introduction**

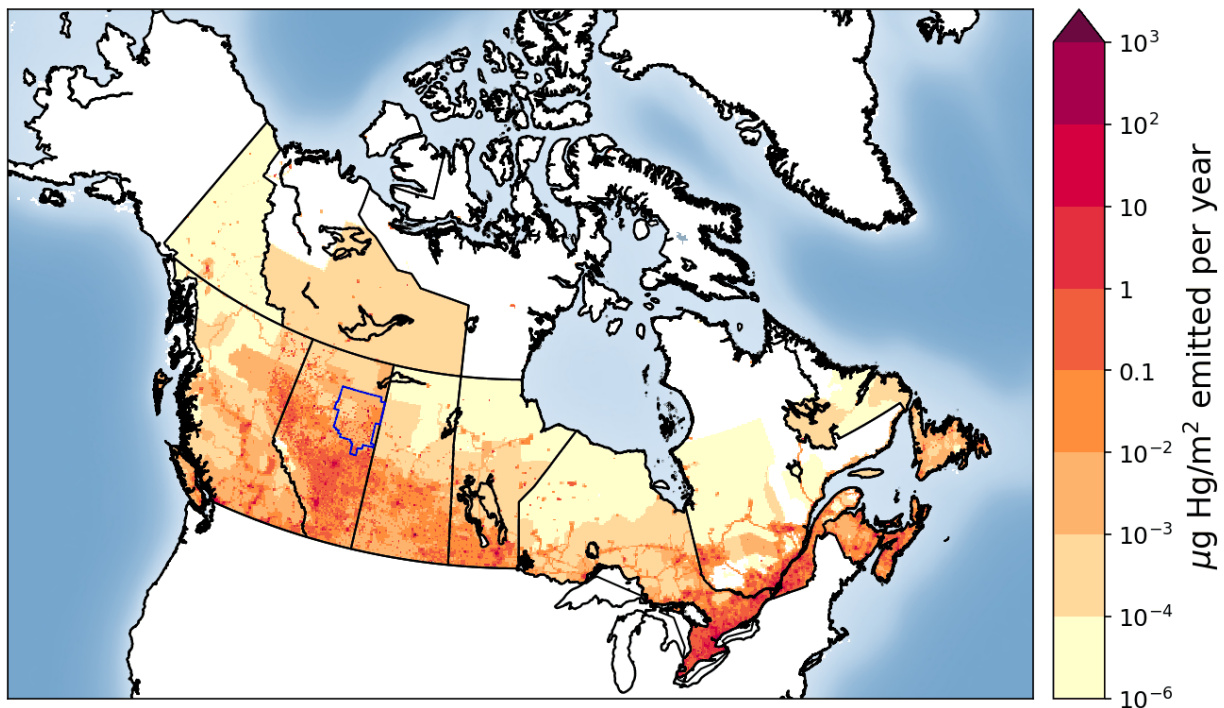
67 Mercury (Hg) is a toxic element that accumulates in fish and mammals near the top of the food  
68 web, including humans (e.g., through consumption of contaminated fish), where it exhibits long-  
69 term toxic effects (UNEP, 2018). Hg is emitted to the atmosphere from geogenic sources such as  
70 volcanoes and the weathering of Hg-containing rocks, anthropogenic sources such as fossil fuel  
71 burning, metal smelting and artisanal gold mining, and through the re-emission of Hg historically  
72 deposited from anthropogenic and natural sources onto soils, surface waters, and vegetation  
73 (UNEP, 2013). Atmospheric Hg exists mainly in three forms: gaseous elemental mercury (Hg(0)  
74 or GEM), gaseous oxidized mercury (gaseous Hg(II); GOM), and particle bound mercury (particle  
75 bound Hg(II); PBM). The sum of GOM and PBM is referred to as total oxidised mercury (TOM)  
76 and the sum of gaseous mercury species (i.e., GEM and GOM) is referred to as total gaseous  
77 mercury (TGM) in this study. GEM/TGM and TOM are better indicators to compare observation  
78 and model estimates of mercury for the purpose of this study, because of speciation uncertainties  
79 associated with the determination of GOM and PBM species (Gustin et al., 2013). Deposition of  
80 atmospheric Hg species by rain and snow (i.e., wet deposition), and by interfacial uptake on  
81 various surfaces such as soils, vegetation, water, and snowpack (i.e., dry deposition) are the  
82 pathways that contribute to Hg loadings in ecosystems. Typically, atmospheric GEM  
83 concentrations are found to be 2-3 orders of magnitude higher (in the low  $\text{ng m}^{-3}$  range) than GOM  
84 and PBM (typically in the lower  $\text{pg m}^{-3}$  range) because GEM is the dominant atmospheric Hg  
85 species emitted to air and the reactivity of the latter (GOM and PBM) leads to efficient dry and  
86 wet deposition removal of these species close to sources. Stability and volatility of GEM results  
87 in its long lifetime in the atmosphere, with six months to one year, allowing for transport and  
88 distribution on a global scale, and re-emission from planetary surfaces (UNEP, 2013).

89

90 On a global scale, dry deposition of GEM by vegetation-uptake over land and wet deposition of  
91 TOM produced by atmospheric oxidation of GEM are the dominant pathways of Hg removal  
92 (Obrist et al. 2016; Wright et al., 2016; Zhou et al. 2021). Primary emissions of GOM and PBM  
93 from industrial sources are an important contributor to dry and wet depositions of Hg on a local to

94 regional scale. Once Hg is deposited to surfaces, it can be reduced and re-emitted back as GEM to  
95 the air and, thus, Hg redistributes and accumulates in the aquatic and terrestrial environments  
96 globally. Hg also inhibits enzymatic processes and reacts with organic compounds. This leads to  
97 the formation of toxic, and bioaccumulating, methyl-Hg, primarily in aquatic systems, which is  
98 the principal cause of a severe neurological syndrome known as “Minamata Disease”. In order to  
99 reduce the amount of Hg released to the environment and limit its exposure to humans, an  
100 international treaty, the Minamata Convention on Mercury, was adopted in 2017 (UN, 2017).

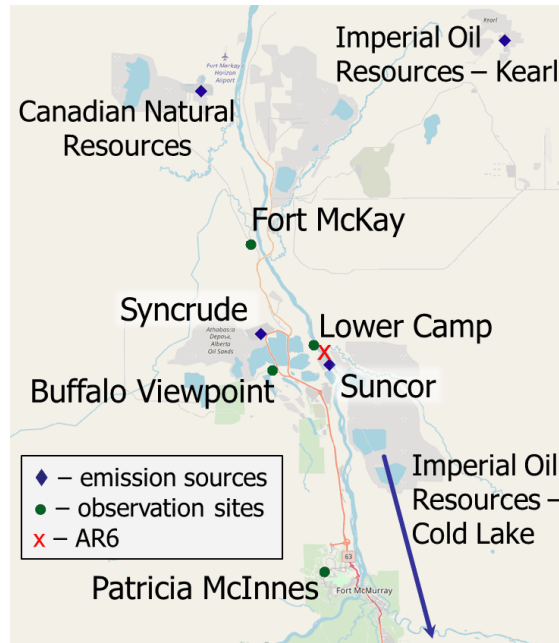
101  
102 Anthropogenic emissions of Hg to air from global sources stand at an estimated 2220 t y<sup>-1</sup> in 2015  
103 (UNEP, 2018). Canadian anthropogenic Hg emissions were estimated at about 4.3 t y<sup>-1</sup> (less than  
104 0.2% of global anthropogenic emissions) in 2015, with an estimated 58% coming from point  
105 sources such as coal-fired power plants and smelters, and 42% from area sources (Zhang et al.,  
106 2018; see Figure 1). Anthropogenic Hg emissions in Canada have declined by 85% from 1990 to  
107 2010 (from ~35 to 5 t y<sup>-1</sup>), with major reductions from sectors such as the non-ferrous metal  
108 mining and smelting (-98%), chemical industries (-95%), waste (-76%), iron and steel industries  
109 (-54%) and electric power generation (-30%) (CMSA, 2016). However, due to the steady increase  
110 in development of the oil sands, the upstream petroleum sector has shown increases in Hg  
111 emissions and accounted for approximately 4.6% of the total Canadian Hg emissions in 2010  
112 (CMSA, 2016).



113  
 114 Figure 1: Spatial distribution of anthropogenic Hg emissions in Canada in 2015 ( $\sim 4.3$  t/y). The  
 115 Athabasca Oil Sands Region is indicated with an approximate rectangular blue shape within  
 116 northeastern Alberta, bordering Saskatchewan.

117  
 118 The Athabasca Oil Sands Region (AOSR) in the northeastern portion of the Canadian province of  
 119 Alberta (see Figure 1) is a zone of extensive natural resource development. The large natural  
 120 deposits of bitumen, a heavy crude oil, contained in a mixture of water and clay (called “oil sands”)  
 121 has led to establishment of large-scale mining and upgrading activities in the area north of Fort  
 122 McMurray, Alberta (AB) (see map Figure 2). Surface mining and in-situ recovery methods are  
 123 used to extract bitumen and then upgrade it to synthetic crude oil (Alexander and Chambers, 2016;  
 124 Larter and Head, 2014). Point source emissions of organics and heavy metals, including Hg,  
 125 originate from mining activities and upgrading facilities in the AOSR. The upgraders are operated  
 126 by the companies Suncor, Syncrude, and Canadian Natural Resources. The upgrading process also  
 127 includes the removal of impurities consisting of sulfur and nitrogen-containing compounds by  
 128 catalytic hydrotreatment, with volatile hydrogen sulfide and ammonia as by-products. Trace metals  
 129 contained in the heavy asphaltene fraction are also removed by either stabilization, rejection, or  
 130 upgrading of asphaltenes (Jia, 2014). The yearly amounts of total Hg emissions from Athabasca

131 oil sands facilities, for the years 2012 to 2015, were between 69 and 25 kg. These annual emissions  
132 exhibited an overall downward trend (for details see Table 1 and Figure 3).



133  
134 Figure 2: Map of the AOSR with the main point sources for Hg emissions from oil sands  
135 developments, and air observation sites. “AR6” marks the approximate midpoint of operations as  
136 defined by Kelly et al. (Kelly et al., 2010).

137  
138 In 2010, Kelly et al., reported increased concentrations of 13 different trace metals including Hg  
139 in the surface waters of the Athabasca River and its tributaries in the oil sands region (Kelly et al.,  
140 2010). Observed concentrations were higher near oil sands operations than away from the potential  
141 sources. Comparison of upstream and downstream data showed consistently higher concentrations  
142 for downstream sites. A similar set of observations was made for Hg in surface snow samples,  
143 more specifically, Hg bound to particulates. Concentrations in accumulated snow collected near  
144 oil sands developments in March averaged 861 ng m<sup>-2</sup> compared to less than 100 ng m<sup>-2</sup> for  
145 background measurements (Kelly et al., 2010). Several oil sands installations were identified as  
146 potential sources for the elevated observations of Hg, but no direct link between sources and  
147 observations was established. Specifically, upgraders were discussed as a source for high Hg levels  
148 in the region. Other potential sources included fly ash, road dust, land clearing and mining  
149 operations.

151 To address the lack of Hg monitoring and attribution of sources, as concluded by Kelly et al.  
152 (2010), several follow-up studies were conducted with the intention to establish a conclusive link  
153 between measured pollutant concentrations and potential sources in the AOSR (Kelly et al., 2010;  
154 Cooke et al., 2017; Kirk et al., 2014; Emmerton et al., 2018; Lynam et al., 2018; Willis et al., 2019;  
155 Willis et al., 2018; Gopalapillai et al., 2019). In addition to water and snow samples, other media  
156 have been investigated, such as air, biota and sediments. Cooke et al. (2017) studied lake sediment  
157 cores sampled from 20 lakes at various distances from oil sands operations, including two of them  
158 in the near vicinity (i.e., within 20 km) of the two major upgrading facilities (Suncor and Syncrude)  
159 within the region (or site AR6 as designated by Kelly (2010)) (Cooke et al., 2017). The cores  
160 provided trace metal data for approximately the past 100-250 years. The cores showed that Hg  
161 concentrations have increased by a factor of 3, reflecting the generally accepted scientific finding  
162 that global Hg has increased 3-fold as a result of anthropogenic activities since the industrial  
163 revolution. No additional increase of Hg concentrations was detected related to the beginning of  
164 oil sands operations in the late 1960s. This contrasts with Kelly et al. (2010) and the follow-up  
165 study by Kirk et al. (2014) that showed higher Hg loadings in the accumulated snowpack and  
166 surface water sampled closer to the mining and upgrading facilities in the AOSR in early spring  
167 (March), mostly consisting of PBM of atmospheric origin. While Hg levels were closely correlated  
168 with other trace metal concentrations originating from oil sands activities such as nickel and  
169 vanadium, no direct causal link with air emissions of Hg, as reported to the National Pollutant  
170 Release Inventory (NPRI), was established. Gopalapillai and coworkers recently reported temporal  
171 trends in snowpack loadings of total Hg (THg) and methyl mercury (MeHg) (and 44 other  
172 elements) (Gopalapillai et al., 2019). Using a composite of snowpack profile samples collected  
173 between 2011 and 2016 and data from previous campaigns, a decrease in THg loadings from an  
174 average of 510 ng m<sup>-3</sup> in 2008 to 175 ng m<sup>-3</sup> in 2016 was found within 8 km from AR6. However,  
175 due to the limited temporal coverage (with measurements for THg starting in 2008), the authors  
176 suggested a need for additional studies to understand the impact of Hg in the AOSR.

177  
178 A recent study by Emmerton et al. (2018) examined lake water samples and related observed Hg  
179 and methyl-Hg concentrations to local geology, watershed conditions, and to oil sands activities,  
180 with the latter only contributing an estimated <2% of the overall Hg deposited (Emmerton et al.,  
181 2018). Long-range transport and biomass burning (i.e., forest fires) were suggested to be the major

182 sources of Hg (Emmert et al., 2018). Similarly, in a recent study of wet deposition data by  
183 Lynam et al. (2018), very low fluxes of Hg deposition were calculated, though the study sites used  
184 (AMS6, the Patricia McInnes observation site shown in Fig. 1) were located further away from  
185 emitters. Results suggested that dry deposition could, instead, be a more important pathway of Hg  
186 removal in the region (Lynam et al., 2018).

187  
188 In an effort to explain the elevated Hg concentrations found in the snowpack and waters near oil  
189 sands mining and upgrading activities, tailings ponds were studied as a potential source of Hg  
190 emissions related to oil sands activities (Willis et al., 2018). However, the water in these ponds  
191 (i.e., the non-recycled portion of process water used to process mined bitumen) were found to be  
192 an insignificant source of THg and MeHg.

193  
194 The above-mentioned studies illustrate recent progress in the ongoing effort to examine the link  
195 between observed concentrations and anthropogenic sources of Hg in the AOSR. However, in  
196 addition to local emissions, multiple other sources of mercury emissions impact the region,  
197 especially forest fires and worldwide anthropogenic and geogenic (contemporary and legacy)  
198 emissions that are atmospherically transported into the region. Owing to the much larger emissions  
199 of Hg from worldwide sources, as compared to Canadian sources, and the long lifetime of Hg in  
200 air, imported Hg accounts for the majority of the Hg burden in Canada (CMSA, 2016), rendering  
201 the assessment of the impacts of domestic Hg emissions challenging using measurements alone.  
202 While Cooke et al. (2017) investigated the history of Hg deposition in lake catchments via the  
203 study of sediment cores, only two lakes sampled were close enough (within 20 km) to oil sands  
204 activities, whereas most sites were 20 to >50 km away from the oil sands facilities.

205  
206 After Hg is emitted to air from oil sands mining and upgrading activities, transport, transformation  
207 and deposition processes determine the distribution and amounts of Hg deposited to environmental  
208 media such as vegetation, soils, and water bodies. 3D process-based predictive atmospheric  
209 composition models include process representations (such as atmospheric transport, chemical  
210 transformations, aerosol particle formation and growth, and wet and dry deposition of gases and  
211 particles) and simulate spatiotemporal distributions of pollutants in air and deposition starting from  
212 emissions (anthropogenic and natural) as inputs. These models provide insight into transport and



213 transformation pathways of pollutants and causal links between emissions and concentrations  
214 observed in environmental media. Models have been applied to study Hg source attribution on  
215 global and regional scales, answering questions such as how much a specific emission source  
216 contributes to local and regional air concentrations and deposition, and how does the pollutant  
217 burden change as industrial activity and related emissions vary (UNEP, 2008; CMSA, 2016;  
218 UNEP, 2018)? Model processes are typically constrained by evaluating simulated pollutant levels  
219 using observation data from ground-based monitoring networks and research campaigns.  
220 Additionally, aircraft measurement data provide observation data on the vertical scale.

221  
222 Wildfires are important sources of Hg in Northwestern Canada and climate change is intensifying  
223 their frequency (Fraser et al., 2018). Biomass burning primarily releases legacy Hg previously  
224 deposited to foliage and soils (Friedli et al., 2001; De Simone et al., 2015). Using multivariate data  
225 analysis, Parsons et al. (2013) determined contribution from local sources (i.e., oil sands activities)  
226 to be minimal as compared to total gaseous Hg concentrations in the air in the AOSR; however,  
227 the authors noted significant episodes of regional forest fires impacting the observed Hg  
228 concentrations in the air during the summer months (Parsons et al., 2013).

229

## 230 **Objectives**

231 Observations of atmospheric Hg in the AOSR are limited to surface air GEM concentrations and  
232 Hg loadings in snow. Summertime wet and dry deposition is not measured. Therefore, measured  
233 estimates of annual Hg deposition in AOSR is currently not possible. Furthermore, a quantification  
234 of the relative importance of different Hg emission sources responsible for Hg loadings in the  
235 AOSR is required to prioritize mitigation actions. The 3D mercury model, Global Environmental  
236 Multiscale - Modelling Air quality and CHemistry – Mercury (GEM-MACH-Hg), was applied to  
237 develop a comprehensive understanding of atmospheric Hg and deposition levels and pathways,  
238 and the role of emissions from Athabasca oil sands activities (particularly from bitumen upgraders)  
239 on the spatiotemporal distribution of Hg deposition in AOSR. This study addresses the following  
240 questions:

- 241 1. How do air concentrations and ecosystem loadings of Hg species in AOSR compare to  
242 other regions in Canada?

- 243 2. What is the level and geographical extent of the contribution of Athabasca oil sands  
244 emissions on Hg in air and deposition?
- 245 3. How does the impact of oil sands development on Hg levels in the region compare with  
246 the impacts of two other major sources of Hg in the region, biomass burning and global  
247 emissions?
- 248 4. What controls the inter-annual variability in Hg levels in AOSR?

249

250 This is the first study that provides a direct connection between Athabasca oil sands Hg emissions  
251 and deposition of Hg in and around the AOSR. A similar approach using the model GEM-MACH-  
252 Hg was previously applied to the assessment of Hg source apportionment at national and global  
253 scales (CMSA, 2016; AMAP/UNEP, 2013; UNEP, 2018).

254

### 255 **The model and emission inputs**

256 GEM-MACH-Hg (Dastoor et al., 2015) is the mercury version of Environment and Climate  
257 Change Canada's 3D process-based operational air quality forecast model GEM-MACH (Global  
258 Environmental Multiscale - Modelling Air quality and Chemistry; Makar et al., 2018; Whaley et  
259 al., 2018). GEM-MACH includes emissions of gases and aerosols, and simulates meteorological  
260 processes, aerosol microphysics, tropospheric chemistry and pollutant dry and wet removal  
261 processes from the atmosphere. In addition, GEM-MACH-Hg includes emissions, chemistry and  
262 dry and wet removal processes of three Hg species (GEM, GOM and PBM) (Dastoor and Durnford  
263 2014; Dastoor et al., 2008; Durnford et al., 2012; Fraser et al., 2018; Kos et al., 2013; Zhou et al.  
264 2021). The recent version of GEM-MACH-Hg, previously applied to the investigation of the  
265 importance of biomass burning emissions to the Hg burden in Canada (Fraser et al., 2018) and the  
266 role of vegetation Hg uptake (Zhou et al. 2021), was used in this study. Oxidation of GEM and  
267 gas-particle partitioning of oxidized Hg species (GOM and PBM) are the main chemical  
268 transformation processes, and dry deposition of GEM, GOM and PBM, and wet deposition of  
269 GOM and PBM are the major removal pathways of Hg in the model. Since observations of  
270 snowpack Hg loadings at the end of the winter season are utilized for model evaluation in this  
271 study, a detailed representation of the air-cryosphere Hg exchange and transformation processes  
272 is important. GEM-MACH-Hg includes a dynamic multilayer air-snowpack-meltwater Hg  
273 parameterization, representing Hg accumulation by precipitation and dry deposition to snowpacks,

274 vertical diffusion and redox reactions in snowpacks, and re-volatilization and meltwater run-off of  
275 Hg species (Durnford et al., 2012). Geospatially distributed global, regional and local emissions  
276 of Hg species (GEM, GOM and PBM) to air from primary geogenic and anthropogenic sources  
277 and re-emissions of previously deposited Hg (legacy Hg) from terrestrial and oceanic surfaces are  
278 included in the model.

279  
280 Three geographical domains were utilized for the model simulations in this study: global, North  
281 America (NA) and AOSR. A geospatial resolution of 10 km was chosen for the NA domain and  
282 its boundary conditions were determined by the global simulations conducted at  $1^{\circ} \times 1^{\circ}$  latitude-  
283 longitude resolution. Model simulations for the AOSR were carried out at a finer geospatial  
284 resolution of 2.5 km for an extended AOSR domain with the approximate midpoint adjacent to the  
285 two largest upgrading facilities (called “AR6”) (Kelly et al., 2010) and extending as far north as  
286 Hay River, NT, and as far south as Red Deer, AB; the approximate western and eastern extents of  
287 the domain are marked, respectively, by Grande Prairie, AB and Flin Flon, MB.

288  
289 Geogenic emissions and re-emissions of legacy Hg in soils and oceans ( $\sim 4200 \text{ t y}^{-1}$ ) emitted as  
290 GEM were distributed as described in Durnford et al., (2012). Wildfire biomass burning Hg  
291 emissions are represented in the model simulations using the FINN (Fire INventory) fire emissions  
292 products (Wiedinmyer and Friedli, 2007; Wiedinmyer et al., 2011) together with vegetation-  
293 specific emission factors (EFs) as described in Fraser et al. (2018). FINN estimated biomass  
294 burning Hg emissions (emitted as GEM) were  $\sim 600 \text{ t y}^{-1}$  globally, and 10.8 (2012), 11.4 (2013),  
295 15.5 (2014) and 11.1 (2015) Mg/y in Canada, and 13.4 (2012), 10.5 (2013), 11.4 (2014) and 9.5  
296 (2015) Mg/y in the US.

297  
298 Contemporary global anthropogenic Hg emissions for 2015 ( $2224 \text{ t y}^{-1}$ ; subdivided into GEM,  
299 GOM and PBM) developed by the Arctic Monitoring and Assessment Programme (AMAP)  
300 (UNEP, 2018) were incorporated into the model for the global scale simulations. For NA and  
301 AOSR domains, GEM-MACH-Hg includes monthly and diurnally varying anthropogenic Hg  
302 emissions in Canada developed by Zhang et al. (2018), based on the NPRI (NPRI) database (2013)  
303 for the major point sources and the 2010 Air Pollutant Emission Inventory (APEI) for the area  
304 sources. Anthropogenic Hg emissions in the United States included in GEM-MACH-Hg were

305 based on the 2011 National Emissions Inventory (NEI) (EPA), described in Zhang et al., (2018).  
306 Total anthropogenic emissions of Hg in Canada, the United States and worldwide were 4.3, 47 and  
307 2224 t y<sup>-1</sup>, respectively. The GEM:GOM:PBM ratio in the total anthropogenic Hg emissions was  
308 approximately 70%:23%:7%.

309  
310 For the oil sands activities related Hg emissions, the model's input consisted only of NPRI-  
311 reported air emissions. Possibility of fugitive dust from the disturbed landscape due to oil sands  
312 activities as a source of particulate-bound Hg emissions was noted by Kirk et al. (2014). Cooke et  
313 al. (2017) were unable to detect Hg from dust emissions in lake sediments. Comparison of modeled  
314 and observed Hg levels conducted in this study allowed an assessment of whether NPRI reported  
315 oil sands emissions and area sources (APEI) in AOSR capture Hg emissions in the region  
316 comprehensively or whether there are other yet undetermined important sources of Hg emissions  
317 such as from fugitive dust in the AOSR.

318  
319 NPRI is a mandatory reporting tool for a wide range of contaminants, including Hg, as prescribed  
320 by the Canadian Environmental Protection Act. Facilities are required to report Hg releases, if total  
321 work hours exceed 20, 000 and if a reporting threshold of 5 kg y<sup>-1</sup> is met for Hg and Hg containing  
322 compounds that were manufactured, processed or otherwise used (includes by-products) or  
323 contained in tailings and waste rock. For the AOSR domain, Hg emissions were updated in the  
324 model from 2012 to 2015 using the NPRI point source Hg emissions data for each year. A summary  
325 of Hg emissions from Athabasca oil sands upgrading facilities (NPRI) for 2012-2015 and temporal  
326 trend from 2004-2017 are available in Table 1 and Figure 3, respectively. Based on NPRI, total  
327 anthropogenic Hg emissions in Canada from the province of Alberta were 605 kg in 2015. Among  
328 these, fossil fuel burning activities such as coal-fired power plants, waste incineration facilities  
329 and other fossil fuel combustion contributed an estimated 221, 120 and 72 kg, respectively, which  
330 represents 68% and, therefore, the bulk of total anthropogenic Hg emissions in Alberta. Iron and  
331 steel production together with the cement industry (emitting 55 and 46 kg, respectively) contribute  
332 another 14% and oil sands upgrading was a minor contributor (~ 25 kg) in 2015.

333

Facility	Latitude	Longitude	2012	2013	2014	2015
Suncor Energy	57.0033	111.466	35	37	0.439	-
Syncrude - Mildred Lake	57.0405	111.619	17	23	30	9.9
Imperial Oil Resources - Cold Lake	54.597	110.399	7	7.4	8.8	11
Imperial Oil Resources - Kearl	57.3969	111.071	-	1.1	4.3	4
<b>Sum of all four sources</b>			<b>59.0</b>	<b>68.5</b>	<b>43.5</b>	<b>24.9</b>

334 Table 1: Athabasca Oil Sands Hg emissions (all in kg yr<sup>-1</sup>) reported to NPRI by oil sands  
 335 processing facilities, and used in the model. For the location of facilities in the AOSR see Figure  
 336 2.

337



338  
 339 Figure 3: Time series of total Hg emissions from oil sands processing facilities in the AOSR. Data  
 340 was compiled from the NPRI database. Numerical values and individual contributions from 2012-  
 341 2017 are available in Table 1.

342

### 343 Model simulations

344 Base model simulations at the three model simulation domains (i.e., global, NA and AOSR) were  
 345 performed using all sources of Hg emissions (as described earlier) and meteorological conditions  
 346 for the respective years from 2010 – 2015 to allow evaluation of modeled air concentrations with  
 347 measured air concentrations for all available years in the AOSR. Snowpack Hg measurements in

348 the AOSR started in 2012. Thus, the model-measurement comparison of snowpack Hg and the oil  
349 sands Hg emissions impact study was conducted for the years 2012-2015.

350

351 Multiple controlled model simulations from 2012-2015 were performed choosing appropriate  
352 geographic domains to assess the relative role of Athabasca oil sands Hg emissions on Hg burden  
353 in the AOSR. The impact of Athabasca oil sands emissions was assessed by zeroing out emissions  
354 of Hg from oil sands facilities in a controlled simulation using the AOSR domain. Contributions  
355 of Hg emissions from biomass burning (in North America) and global anthropogenic sources to  
356 the AOSR Hg levels were obtained by zeroing out emissions from these sources in controlled  
357 simulations on North America and global model domains, respectively. Source apportionment of  
358 the anthropogenic Hg deposition from worldwide sources was conducted using a series of global-  
359 scale controlled simulations by zeroing out anthropogenic Hg emissions in different source  
360 regions. In addition, controlled model simulations were performed to estimate the individual  
361 influences of meteorology, biomass burning emissions and oil sands emissions on the interannual  
362 variations in Hg deposition in the AOSR by successively adding these three temporal changes in  
363 2013-2015.

364

### 365 **Mercury observations in the AOSR**

366 Simulated air concentrations and deposition of Hg were evaluated with observations of Hg in air  
367 and snowpack in the AOSR. These measurements were recorded with instruments deployed for  
368 air quality monitoring purposes and to study the atmospheric deposition of Hg species in the AOSR  
369 (Parsons et al., 2013; Kirk et al. 2014; Gopalapillai et al., 2019). Air measurements were carried  
370 out at three sites in the AOSR: Patricia-McInnes (2010-2018), Fort Mackay (2014-2018), and  
371 Lower Camp (2012-2014). Measurements were made using Tekran 2537 Hg analysers for GEM,  
372 and Tekran 1130/1135/2537 systems for speciated Hg (GOM and PBM) fitted with PM<sub>2.5</sub> and  
373 PM<sub>10</sub> inlets (see map in Figure 2 for equipment placement and Figure 4-6 for data). Standard  
374 operating procedures were provided by the Canadian Atmospheric Mercury Measurement  
375 Network (CAMNet, (Steffen and Schroeder, 1999)). Air measurements of oxidized Hg  
376 concentrations were carried out at only one site near Fort McKay in 2015 (Parsons et al., 2013).  
377 Since Hg deposition to snow is mainly derived from the ambient oxidized Hg concentrations,

378 observations of snowpack Hg loadings provide additional constraint for modeled oxidized Hg  
379 concentrations in air.

380  
381 Snow samples were collected from 2012 to 2015 at 454 sites located at varying distances from the  
382 major upgrading facilities (<1-231 km) to estimate total seasonal Hg loadings in surface snow in  
383 the AOSR (Gopalapillai et al., 2019; Kirk et al., 2014). Specifically, 90 (2012), 86 (2013), 140  
384 (2014) and 138 (2015) samples were obtained from sites located close to the AOSR emission  
385 sources (< 25 km) and at background sites further away from sources (> 120 km). Sample  
386 collection was carried out in early to mid-March of each year at approximate maximum snowpack  
387 depth based on Environment and Climate Change Canada's National Climate Data and  
388 Information Archive historical snow accumulation data (GoC, 2019). Kirk et al. (2014) employed  
389 ultra-clean handling and analysis protocols while taking care to avoid local contamination from  
390 transportation since sites were accessed by helicopter and snowmobile. Mercury analysis in the  
391 snow was carried out using cold vapour atomic fluorescence spectroscopy (Willis et al., 2018; Kirk  
392 et al., 2014; EPA, 1996; Bloom and Crecelius, 1983). The determined snowpack Hg loading at the  
393 end of the winter season represents lower limit of the net wintertime dry and wet deposition of Hg.  
394 Hg deposited to snowpacks is partially reduced and re-volatilized to the air and lost during intra-  
395 seasonal snowpack melting. Summertime measurements of Hg deposition by scavenging in rain  
396 and direct uptake by vegetation, soils and waters were unavailable for model evaluation.

397

## 398 **Results and Discussion**

### 399 **Evaluation of model simulated mercury concentrations in air**

400 GEM-MACH-Hg has been extensively evaluated with comprehensive worldwide (including  
401 Canada) observations, inter-compared with other Hg models, and applied to mercury assessments  
402 in previous studies (Angot et al., 2016; Bieser et al., 2017; Dastoor et al., 2008; Dastoor and  
403 Durnford, 2014; Durnford et al., 2010; Durnford et al., 2012; Fraser et al., 2018; Kos et al., 2013;  
404 Travnikov et al., 2017; Zhou et al. 2021; AMAP 2013; CMSA, 2016; UNEP, 2018). Model  
405 evaluation of ambient Hg in the AOSR is presented in this study. Figures 4-6 provide a comparison  
406 of simulated (blue trace) and observed (red trace) daily averaged TGM concentrations in air at the  
407 three observation sites (Figure 4: Patricia McInnis, 2010-2015; Figure 5: Lower Camp, 2012-2014;  
408 and Figure 6: Fort McKay, 2014-2015), and how the model captured biomass burning events

409 (BBE) (green traces show modeled biomass burning contributions to TGM concentrations). While  
410 some observations are incomplete (e.g., June 2013, Patricia McInnis), the data provide a detailed  
411 picture of TGM surface concentrations near oil sands activities (see Figure 2 for details). In  
412 general, data from all three observation sites and model simulation results agreed well with an  
413 average squared Pearson correlation coefficient of 0.6, and measured and modeled median TGM  
414 concentrations ( $\pm$  standard deviation) of  $1.34 \pm 0.21$  and  $1.39 \pm 0.17$  ng m<sup>-3</sup> (2011-2015) at Patricia  
415 McInnis,  $1.36 \pm 0.17$  and  $1.36 \pm 0.18$  ng m<sup>-3</sup> (2013) at Lower Camp and  $1.22 \pm 0.23$  and  $1.33 \pm 0.19$   
416 ng m<sup>-3</sup> (2014-2015) at Fort Mckay, respectively. The model captured the observed seasonal cycle  
417 (typical in the northern hemisphere) with spring maxima and fall minima, shaped mainly by  
418 surface fluxes of Hg such as the dominance of re-emission fluxes of Hg from snow in winter and  
419 spring, and uptake of Hg by vegetation in summer and fall (Zhou et al. 2021). Transport of Hg  
420 from biomass burning (i.e., wildfires) events in northern and western Canada yielded distinct Hg  
421 concentration peaks in TGM concentrations in the AOSR (Figures 4-6). For 2011, biomass burning  
422 provided a large contribution to overall TGM concentrations, which peaked during these events at  
423 Patricia McInnis; however, no concurrent observations were available for the months of May and  
424 June. During the large wildfire events in 2012 and 2015 (June-July), daily averaged TGM  
425 concentrations were generally  $< 2.5$  ng m<sup>-3</sup>, which were accurately reproduced by the model.  
426 However, as shown in Figure 5 for the Lower Camp site in August 2013, there are discrepancies  
427 between modeled and observed wildfire events. The impacts of biomass burning emissions on Hg  
428 burden in Canada and the uncertainties in wildfire Hg emissions associated with the  
429 characterization of wildfire events and emission levels using satellite and field data were described  
430 in a previous study (Fraser et al., 2018). Low TGM concentration events in winter and early spring,  
431 such as those in March 2014 at Patricia McInnis, were typically associated with clean air masses  
432 coming from the Arctic in AOSR. Model-measurement agreement of TGM levels in the air is  
433 within the respective model and measurement uncertainties and indicates that reported Hg  
434 emissions from AOSR facilities are reasonable.

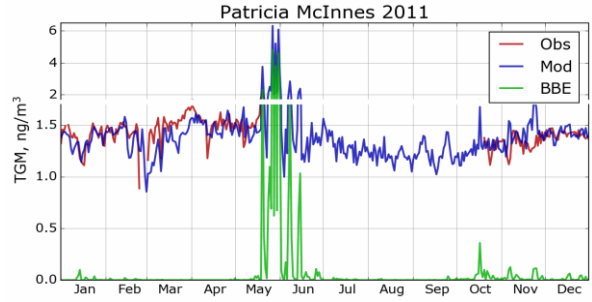
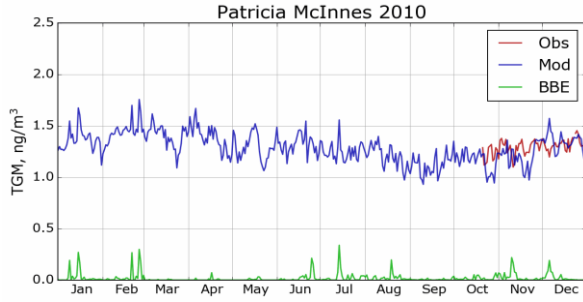
435  
436 GOM and PBM observations were conducted at Fort McKay (a region dominated by natural boreal  
437 forest) using PM<sub>2.5</sub> (captures particle sizes  $< 2.5$   $\mu$ m) and PM<sub>10</sub> (captures particle sizes  $< 10.0$   $\mu$ m)  
438 inlets in AOSR for 2015, but significant measurement data gaps were present particularly in winter  
439 and spring. Observed annual average concentrations were  $1.02 \pm 2.59$  (GOM) and  $3.47 \pm 4.79$  pg



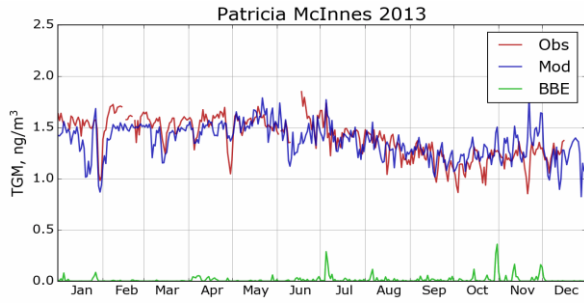
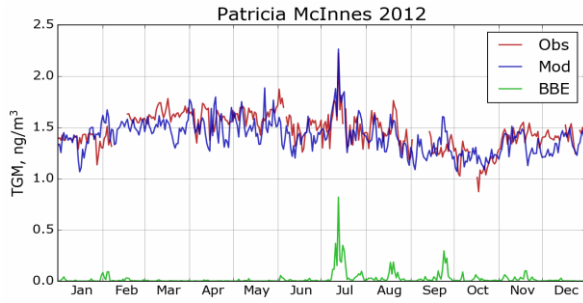
440  $\text{m}^{-3}$  (PBM) using the  $\text{PM}_{2.5}$  inlet, and  $0.60 \pm 1.11$  (GOM) and  $4.25 \pm 8.23$   $\text{pg m}^{-3}$  (PBM) using the  
441  $\text{PM}_{10}$  inlet in 2015; these observations suggest a dominance of PBM in fine particles ( $< 2.5 \mu\text{m}$ )  
442 at the Fort McKay site (17 km Northwest of AR6). The model simulated and observed average  
443 TOM air concentrations and standard deviation ( $\pm 1\sigma$ ) in 2015 were  $4.74 \pm 5.06$   $\text{pg m}^{-3}$  and  $5.74 \pm$   
444  $7.20$   $\text{pg m}^{-3}$ , respectively; observed data from both inlets was combined to reduce measurement  
445 gaps. Episodes of high concentrations of particulate Hg (up to  $72.9$   $\text{pg m}^{-3}$ ), occurring  
446 predominantly on coarse ( $> 2.5 \mu\text{m}$ ) particles, , that were absent in the modeled PBM  
447 concentrations were observed in March. The sources of coarse particles in the AOSR are currently  
448 unknown, but fugitive dust from pet coke piles and roads as a result of oil sands mining activities  
449 was suggested by Gopalapillai et al. 2019. It should be noted that uncertainty of a factor of 2 or  
450 higher with oxidized Hg measurements has been reported (Kos et al., 2013; Gustin et al. 2015).  
451 Comparable average GOM and PBM concentrations of  $1.89 \pm 8.31$  and  $3.82 \pm 4.90$   $\text{pg m}^{-3}$  (mean  
452  $\pm 1\sigma$ , 2009-2011), respectively, have been measured at a site 8 km from a coal-fired power plant  
453 in Genesee, AB (about 500 km southwest of Fort McMurray). Seasonal cycles at the two sites  
454 (Fort McKay and Genesee) were similar, with TOM maxima in May-June. Since Hg deposition to  
455 snow is primarily driven by the uptake of ambient oxidized Hg species in snowfall and snowpack,  
456 the robustness of model simulated oxidized Hg in air was further tested by comparing modeled  
457 snowpack Hg loadings with measurements (see next section).

458

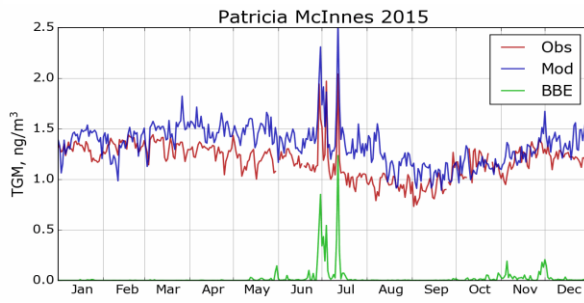
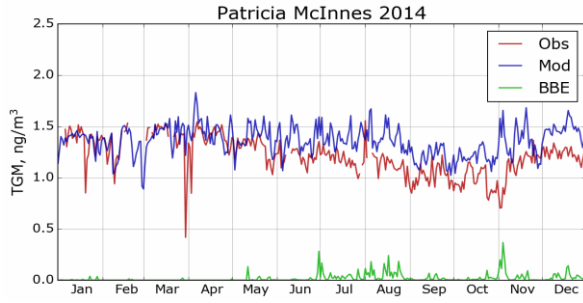
459



460



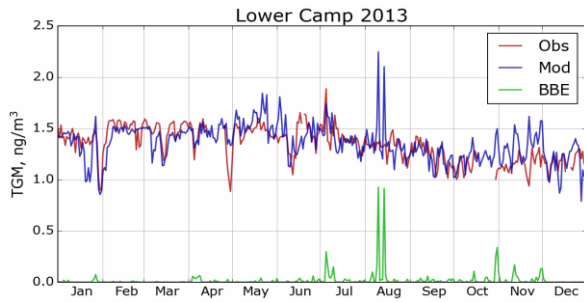
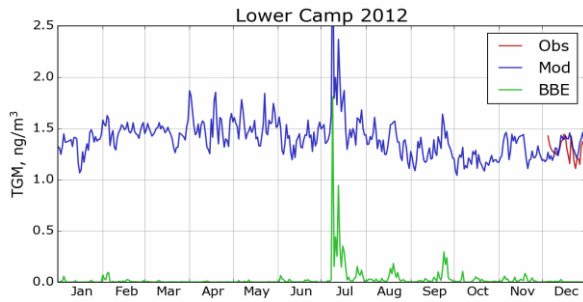
461

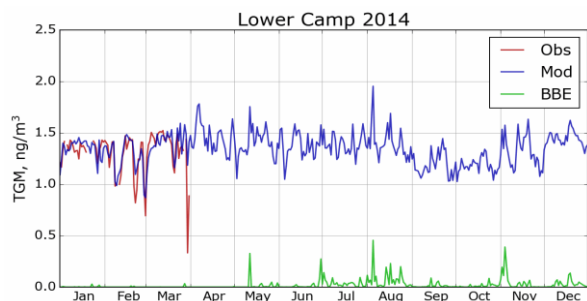


462 Figure 4: Simulated and observed daily averaged surface air TGM concentrations in AOSR for the  
 463 site Patricia-McInnes (2010—2015). Obs – observations; Mod – model estimation; BBE –  
 464 modeled biomass burning contributions. Note the larger range of the y-axis to plot the strong  
 465 biomass burning event in May and June of 2011.

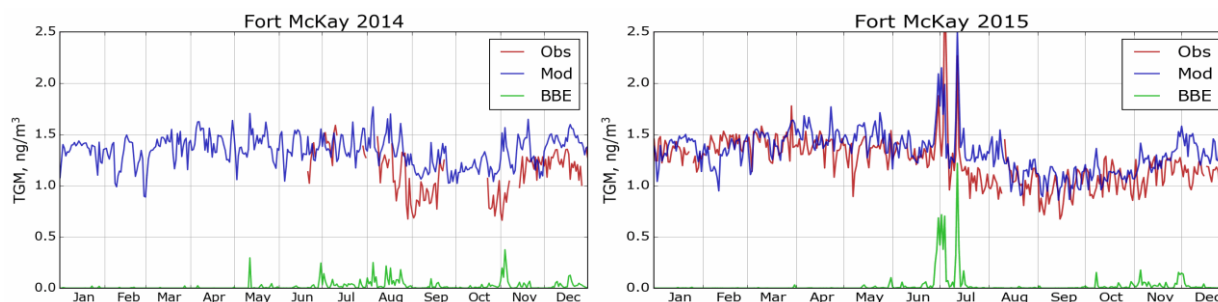
466

467





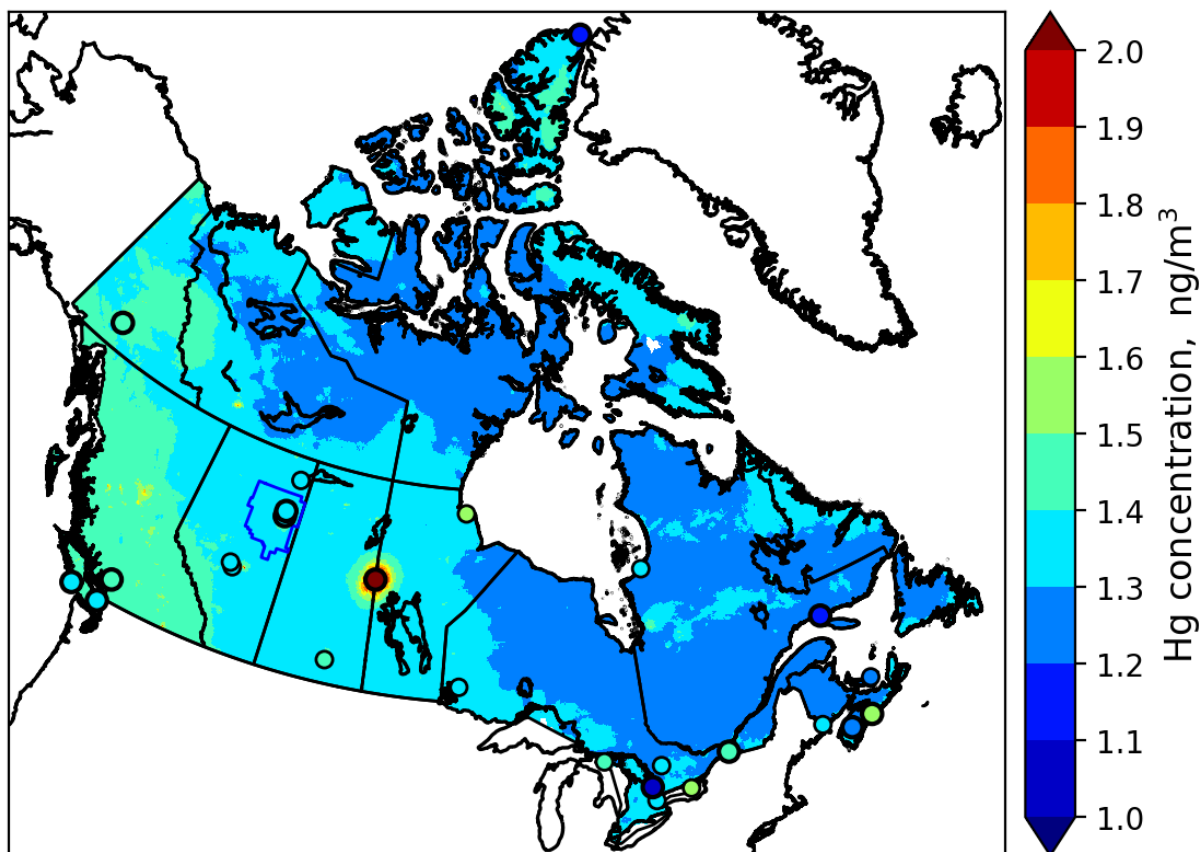
468  
 469 Figure 5: Simulated and observed surface air TGM concentrations in AOSR for the site Lower  
 470 Camp (2012—2014). Obs – observations; Mod – model estimation; BBE – modeled biomass  
 471 burning contribution.  
 472



473  
 474 Figure 6: Simulated and observed surface air TGM concentrations in AOSR for the site Fort  
 475 McKay (2014 and 2015). Obs – observations; Mod – model estimation; BBE – modeled biomass  
 476 burning contributions.  
 477

478 For the purpose of comparing ambient GEM concentrations in the AOSR with other Canadian  
 479 regions, Figure 7 provides a map of modeled annual average surface air Hg concentrations of GEM  
 480 for Canada in 2013. In general, model estimated surface air GEM concentrations agreed well with  
 481 available observations (in circles), including western Canada, the Pacific coast, and the AOSR.  
 482 There is a general gradient in GEM concentrations from higher concentrations in the west (1.5 ng  
 483 m<sup>-3</sup>) to lower concentrations in the east (1.3 ng m<sup>-3</sup>). The average air concentrations of GEM in  
 484 the AOSR (1.40 ng m<sup>-3</sup>, 2012-2015) reflected the background GEM levels in Canada. The  
 485 simulated large-scale pattern in GEM concentrations is consistent with, and reflects, a dominant  
 486 role of trans-Pacific transport of GEM from East Asian Hg sources into Canada and the high  
 487 Arctic. GEM concentrations are slightly higher in major urban centres and regions of current and  
 488 past anthropogenic activities such as energy production from coal-fired power plants and mining.  
 489 The hotspot in Figure 7 near the Saskatchewan/Manitoba border is the former copper-zinc smelter

490 near Flin-Flon, MB, which ceased operations in 2010 (Ma et al., 2012). The soils in the  
491 surrounding region remain heavily contaminated with Hg. The re-emission of accumulated legacy  
492 mercury in soils (Eckley et al., 2013) is responsible for the highly elevated GEM concentrations  
493 in air.  
494



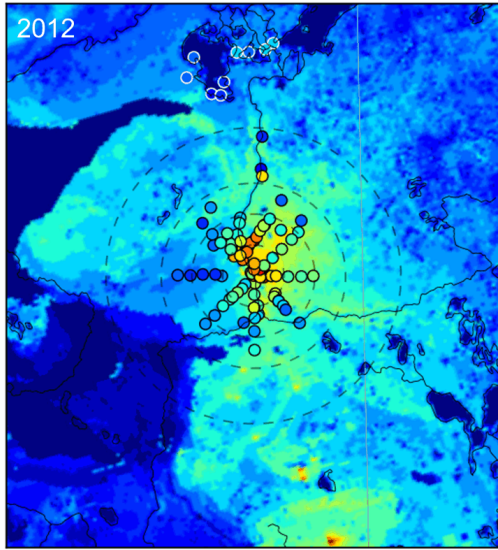
495  
496 Figure 7: Model simulated spatial distribution of annual average surface air GEM concentrations  
497 in Canada in 2013; colors in circles show observed concentrations for 2013 (large circles) and  
498 previous years (small circles).  
499

#### 500 **Evaluation of model simulated mercury accumulation in snow**

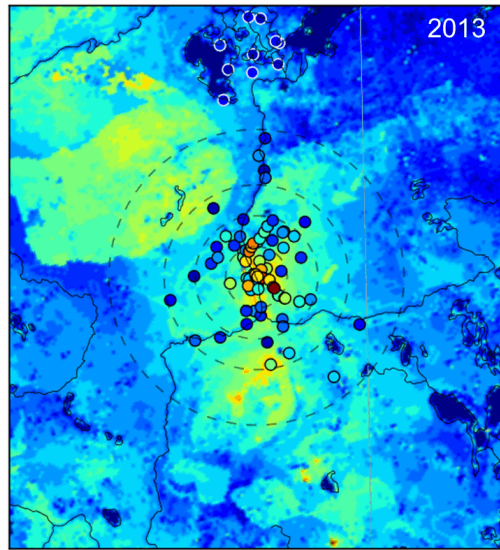
501 Figure 8 compares total Hg loadings in snow simulated by the model with observations (in circles)  
502 at the end of winter for years 2012-2015 in the AOSR. Cooke et al., (2017) used dated lake  
503 sediment cores to reconstruct deposition trends and anthropogenic enrichment in the region, but  
504 several correction factors needed to be applied to estimate Hg deposition fluxes and only two lakes  
505 were cored in the direct vicinity of oil sands operations. By comparison, seasonal snowpack Hg

506 data provide the distribution of net total Hg deposition in the region with a large number of  
507 sampling sites a short distance (< 25 km) away from sources. However, it should be noted that Hg  
508 deposition in the snow is partially reduced and reemitted as well as adsorbed in surface soils due  
509 to diffusion and intra-seasonal melt; therefore, snowpack Hg represents the lower limit of net  
510 wintertime deposition. Observations at the sampling sites close to sources had the highest  
511 snowpack Hg loadings with decreasing concentrations as one moves further away from the  
512 immediate source region; the same spatial pattern was predicted by the model, and is most evident  
513 for the years with the largest emissions (2012 and 2013; Figure 8). Snow Hg contents at the  
514 background sites in the Peace Athabasca Delta region in the north were significantly lower, which  
515 was also well reproduced by the model. The figure shows high spatiotemporal variability in snow  
516 Hg loadings, which are related to changes in meteorological factors as well as oil sands emissions  
517 (as discussed later). The decline in both snowfall amounts and oil sands emissions led to lower  
518 snow Hg loadings in 2014 and 2015. Figure 9 shows the model simulated average snow depths in  
519 the AOSR and the observed depths at the Mildred Lake site close to the Syncrude upgrader. The  
520 model simulates snow amounts and interannual variations accurately. The model-estimated  
521 seasonal snow accumulations were 62, 183, 104 and 71 cm between October to May in 2012, 2013,  
522 2014 and 2015, respectively. An intense intra-seasonal melting event at the end of February was  
523 predicted by the model in each year, which is inline with observations. The largest melting event  
524 occurred in 2015, which caused over half of the snow accumulation to melt, and, thus, loss of half  
525 of seasonal snowpack Hg loadings. Modeled snow Hg loadings are in agreement with Gopalapilla i  
526 et al. (2019), who reported a temporal decrease in snow Hg loadings near-field (< 8 km from AR6),  
527 from an average load of 510 ng/m<sup>2</sup> in 2008 to 175 ng/m<sup>2</sup> in 2016. Relative importance of inter-  
528 annual changes in meteorological conditions and oil sands emissions to wintertime Hg deposition  
529 is discussed a later section.

530

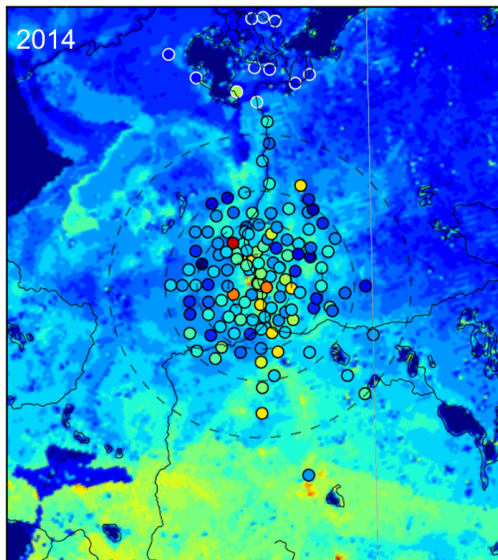


0 0.04 0.08 0.13 0.2 0.3 0.4 0.6 1 1.4  
Hg accumulation in snow,  $\mu\text{g}/\text{m}^2$

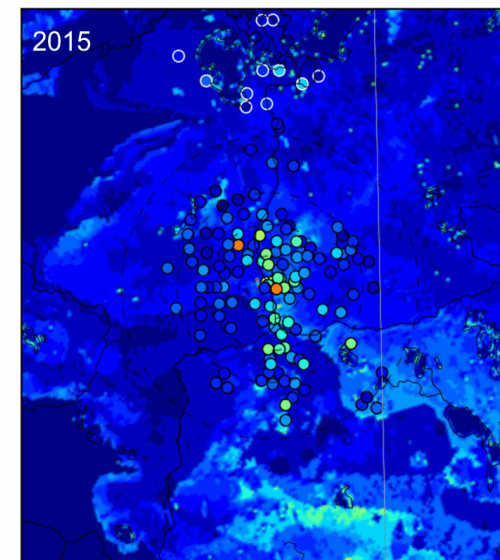


0 0.04 0.08 0.13 0.2 0.3 0.4 0.6 1 1.4  
Hg accumulation in snow,  $\mu\text{g}/\text{m}^2$

531



0 0.04 0.08 0.13 0.2 0.3 0.4 0.6 1 1.4  
Hg accumulation in snow,  $\mu\text{g}/\text{m}^2$



0 0.04 0.08 0.13 0.2 0.3 0.4 0.6 1 1.4  
Hg accumulation in snow,  $\mu\text{g}/\text{m}^2$

532

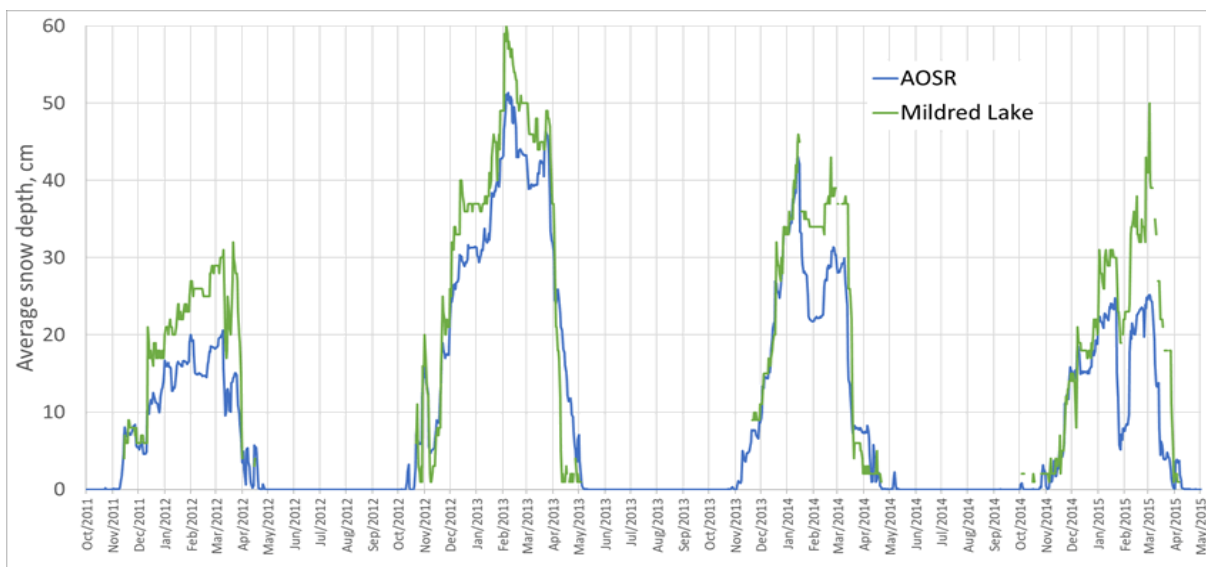
533

534

535

Figure 8: Seasonally accumulated Hg loadings in snow in AOSR from 2012 to 2015: modeled (background map) and observed values (colors in circles). Circles radii: 25, 50, 75, 120 km.





536  
 537 Figure 9: Daily averaged model simulated (blue) and observed snow depths (green) (cm) in 2012-  
 538 2015 in the AOSR. Modeled values are averaged over the entire AOSR domain and the observation  
 539 site is Mildred Lake, Alberta, a few km east of the Syncrude oil sands upgrader.

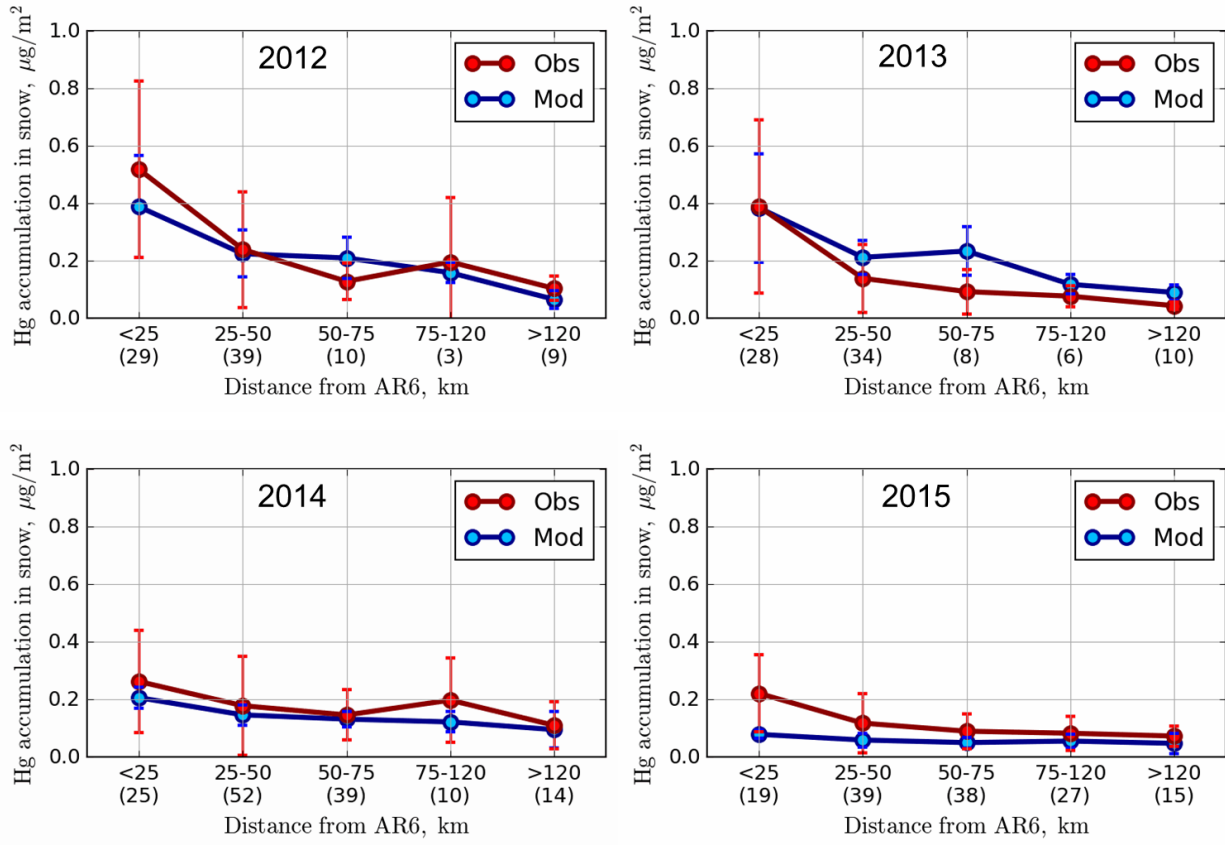
540  
 541 Figure 10 compares average modeled and observed snow Hg loadings at the sampling locations  
 542 within 25 km, 25-50 km, 50-75 km, 75-120 and > 120 km distances from AR6. Inter-annual  
 543 changes in meteorology and oil sands emissions led to decreases in total Hg loads from  $0.52 \pm 0.21$   
 544 to  $0.22 \pm 0.09 \mu\text{g m}^{-2}$  within 25 km of AR6 (from 2012 to 2015) in the snowpack for observation  
 545 and from  $0.39 \pm 0.21$  to  $0.08 \pm 0.06 \mu\text{g m}^{-2}$  for model estimates sampled at sites. The snow Hg  
 546 loadings of up to  $0.7 \mu\text{g m}^{-2}$  were simulated by the model in the immediate vicinity of Hg emitting  
 547 sources for 2012 (Figure 8). Emitted amounts of Hg from oil sands facilities were reported to the  
 548 NPRI with the caveat that not all emissions, e.g., emissions of mercury that are part of fugitive  
 549 dust releases, are captured by the inventory. Brief episodes of Hg on larger particles ( $2.5\text{-}10 \mu\text{m}$   
 550 size) were observed at Fort McKay in late winter, likely originating from fugitive dust in the  
 551 AOSR. These possible sources of Hg emissions and related deposition (in the vicinity of sources)  
 552 were not included in the model. At > 120 km from AR6, snowpack loadings were very low for all  
 553 years at  $< 0.1 \mu\text{g m}^{-2}$  with small inter-annual variability, and indicate background Hg  
 554 concentrations at this distance.

555  
 556 While the strong decrease away from the source is mirrored in Figure 10 for the years 2012 and  
 557 2013 (dropping from about  $0.4 \mu\text{g m}^{-2}$  at sites located <25 km from AR6 to  $< 0.1 \mu\text{g m}^{-2}$  at sites >

558 120 km away), the weaker signature from Figure 8 for the years 2014 and 2015 is more clearly  
559 represented in Figure 10, consistent with declines in reported oil sands emissions (see Table 1 and  
560 Figure 3). Modeled snow Hg loadings closer to the oil sands sources were lower compared to  
561 observed values in 2015. A sensitivity model simulation was conducted for 2015 by replacing  
562 NPRI reported Hg emissions from oil sands facilities in 2015 with 2014 values. The sensitivity  
563 model simulation matched the observed Hg loadings in the snow in 2015 at all distances; these  
564 results suggest that either NPRI Hg emissions from oil sands facilities were slightly under-  
565 represented or there was an unaccounted area source (such as from fugitive dust) of Hg in 2015.

566  
567 Model estimates and observations agreed well for all distances evaluated, and demonstrate the  
568 model's ability in correctly simulating the impacts of changes in Hg emissions and  
569 physicochemical processes in the cryosphere. The high variability in the observed snowpack data  
570 within 50 km of AR6 indicates that there are likely other local sources around mining facilities  
571 that impact local deposition (such as fugitive dust from coke pile and roads). However, modeled  
572 estimates at sampling locations agreed with observed snow Hg loadings within one standard  
573 deviation, and suggest that unaccounted sources of Hg do not have a significant impact on  
574 deposition in the AOSR, likely due to their episodic nature as suggested by observed ambient  
575 concentrations of particle-bound mercury.





576

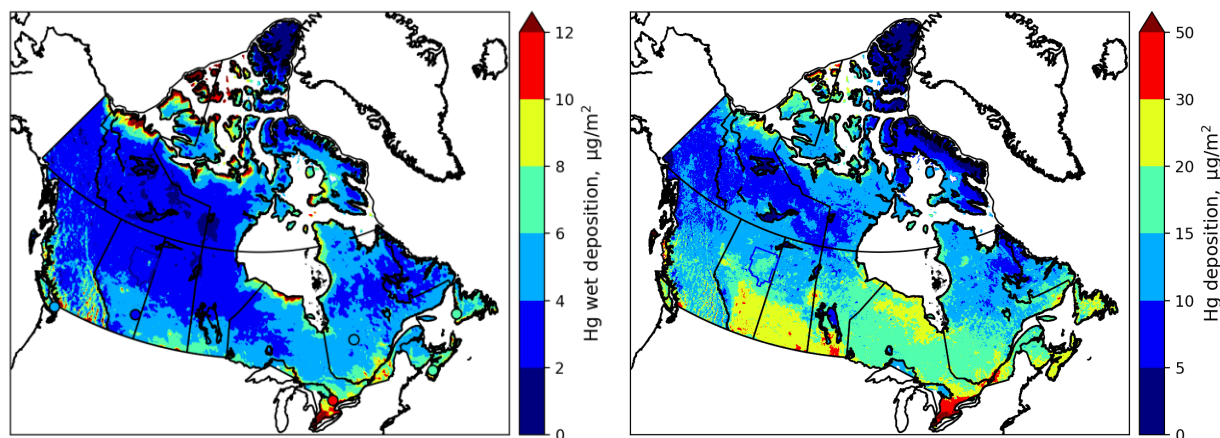
577

578 Figure 10: Average modeled ( $\mu\text{g m}^{-2}$ ; blue) and observed ( $\mu\text{g m}^{-2}$ ; red) end of winter Hg loadings  
 579 in snowpack within 25 km, 25-50 km, 50-75 km and 75-120 and > 120 km distances from AR6  
 580 along with  $\pm$ one standard deviations. Modeled accumulated Hg in the snow was sampled at the  
 581 observation sites. Numbers in parentheses provide number of observation sampling sites in each  
 582 distance cluster.

583

584 Comparison of modeled annual wet and total deposition (wet plus dry deposition) fluxes of Hg in  
 585 the AOSR with other locations in Canada is presented in Figure 11 for 2013. In general, spatial  
 586 distributions of wet and total deposition fluxes followed patterns of precipitation (high in the east,  
 587 south and mountainous regions of Canada), industrial activities (high in southern Canada),  
 588 vegetation density (boreal and temperate forests) as well as Hg transport from the US (higher in  
 589 the east). Figure 11 shows good agreement with observed wet deposition fluxes (noted in circles)  
 590 in coastal (Saturna Island, BC), rural (Southern Alberta) and urban areas (Egbert, ON). While  
 591 direct measurements of annual total deposition fluxes are not available, the distribution of Hg  
 592 deposition fluxes in Canada was found to be consistent with Canada-wide lake sediment inferred

593 deposition fluxes (Muir et al. 2009). Average annual total deposition fluxes in the AOSR were  
594 16.9, 15.7, 18.3 and 17.5  $\mu\text{g m}^{-2}$  in 2012, 2013, 2014 and 2015, respectively, slightly higher than  
595 in the other regions of northern Alberta ( $\sim 14 \mu\text{g m}^{-2}/\text{y}$ ) and lower than average Hg deposition flux  
596 in southern Alberta ( $\sim 25 \mu\text{g m}^{-2}/\text{y}$ ). The highest deposition up to  $80 \mu\text{g m}^{-2}$  occurred in southern  
597 Ontario in Canada due to the presence of local anthropogenic mercury emissions in these regions.

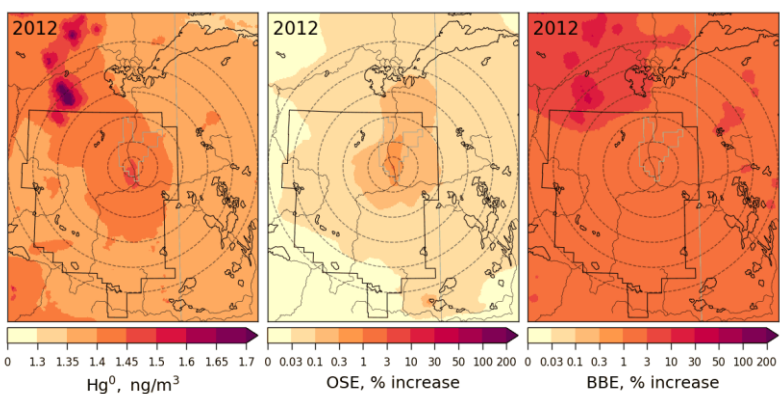


598  
599 Figure 11: Model simulated and observed annual Hg wet deposition for 2013 (left) (colors in  
600 circles show observed wet deposition for 2013) and simulated annual total Hg deposition (right)  
601 (wet plus dry deposition) in Canada for 2013.

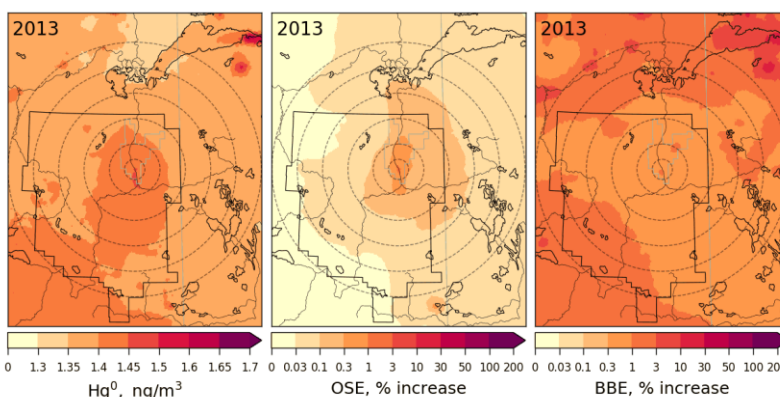
602  
603 **Impacts of oil sands developments and wildfires on mercury levels in air and deposition**  
604 Employing GEM-MACH-Hg, the impacts of Hg emissions from oil sands developments in the  
605 AOSR on surface air concentrations of Hg species (i.e., GEM and TOM), snowpack Hg loadings,  
606 and annual Hg deposition were investigated for the years 2012-2015. Since Northwest Canada is  
607 a region of high wildfire activity (Fraser et al. 2018), the relative role of Hg emissions from  
608 biomass burning in North America on the Hg burden in the AOSR was also examined.

609 Figures 12 & 13 provide spatial distributions of simulated annual average surface air  
610 concentrations of GEM (globally transported and the dominant ambient Hg species) and TOM  
611 (regionally transported and efficiently deposited Hg species) (left panels) for the years 2012 to  
612 2015 along with their contributions (as % increases) from oils sands emissions (OSE, middle  
613 panels) and biomass burning emissions (BBE, right panels) in the AOSR and the surrounding  
614 region. GEM air concentrations were  $1.4 \text{ ng m}^{-3}$  in the AOSR in 2012-2015, which is within the  
615 range of GEM concentrations observed in Alberta (i.e.,  $1.2\text{-}1.5 \text{ ng m}^{-3}$  in 2012). While annual

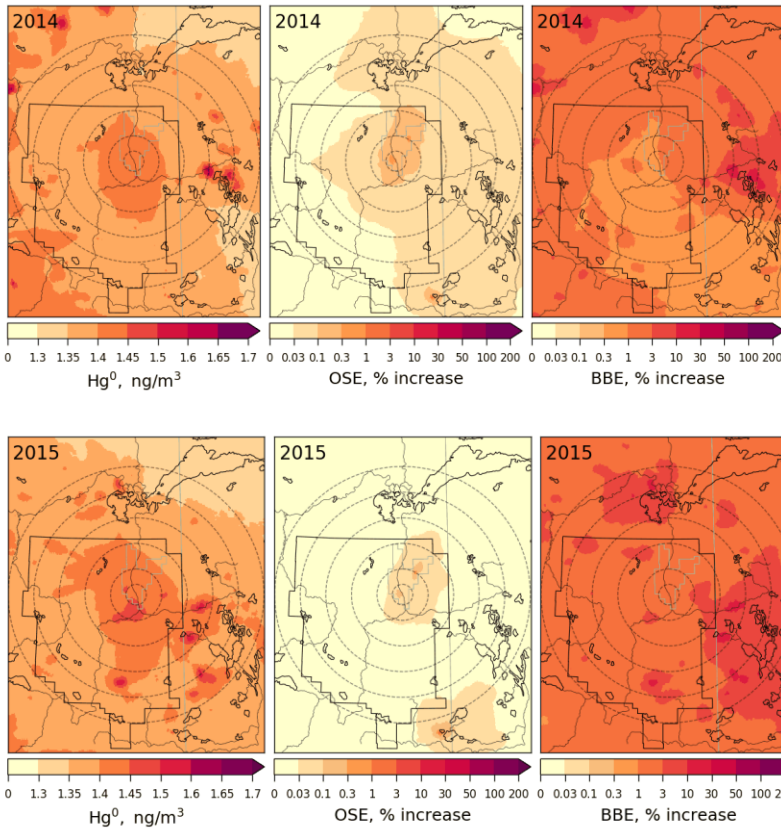
616 average GEM concentrations were slightly elevated close to the major upgraders (> 1.5 within 5  
 617 km vs 1.4 ng m<sup>-3</sup> 200 km away from AR6) in the AOSR, GEM concentrations were found to be  
 618 elevated up to 1.8 ng m<sup>-3</sup> in surrounding regions of the AOSR due to local wildfires in 2012-2015.  
 619 Since the lifetime of GEM in the air is between 0.5-1 year, GEM concentrations are largely driven  
 620 by global transport in the AOSR (and Canada) with only minor contributions from local emissions.  
 621 Oil sands emissions increased atmospheric GEM concentrations up to 2.3% in 2012 and 2013, and  
 622 negligibly (up to 0.9%) in low OSE years 2014-2015, only very close to the upgraders (i.e., within  
 623 2.5 km). Wildfire activities are highly variable from year to year, and can significantly impact  
 624 GEM concentrations in the AOSR in summertime (Fraser et al. 2018). Biomass burning  
 625 contributed to 1.0-2.2% increases in average GEM concentrations in and around the AOSR (Figure  
 626 12, right panels), making biomass burning a more important source of GEM than OSE in the  
 627 region. Strong regional biomass burning events led to large increases in GEM concentrations of  
 628 up to 35% (2012-2015) in the AOSR and the surrounding regions.



629



630



631

632

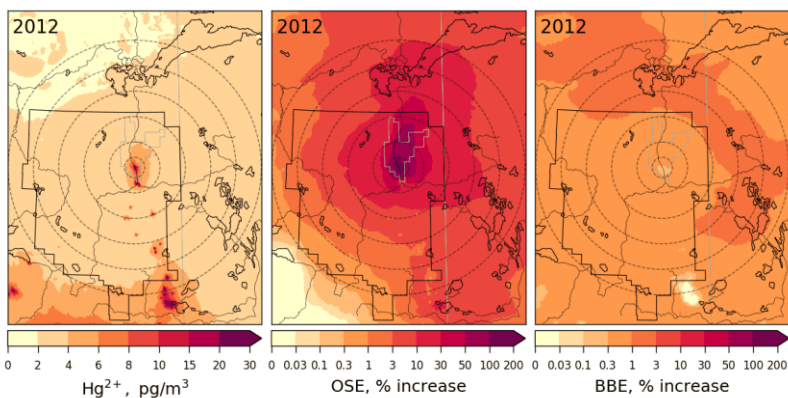
633 Figure 12: Annual average surface air concentration of GEM (left) and concentration enrichments  
 634 (%) due to Hg emissions from Athabasca oil sands operations (OSE, middle) and biomass burning  
 635 in North America (BBE, right) for the years 2012 to 2015. The AOSR is marked as an approximate  
 636 rectangle, and concentric distance circles are at 20, 50, 100, 150, 200 and 250 km from AR6.

637

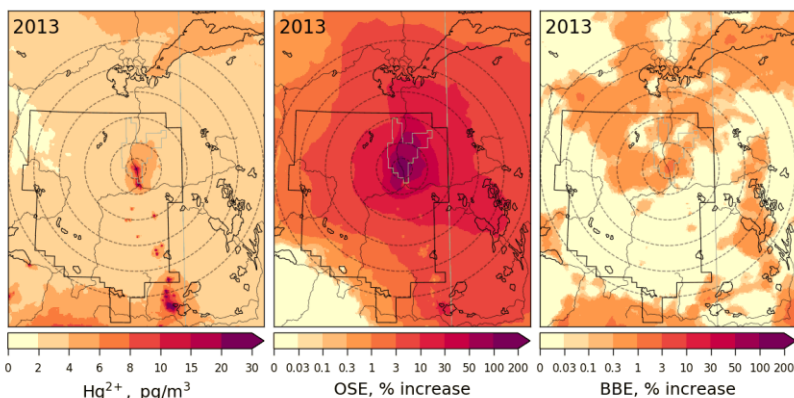
638 While average surface air TOM concentrations in the AOSR were only  $3.3 \text{ pg m}^{-3}$  (consistent with  
 639 observations), hot spots were modelled in the immediate vicinity of the major upgraders ( $> 25 \text{ pg}$   
 640  $\text{m}^{-3}$  within 5 km from AR6 in 2012-2013) in the AOSR (Figure 13, left panels). In 2014-2015,  
 641 TOM concentrations around AR6 were about half of 2012-2013 ( $12 \text{ pg m}^{-3}$ ), consistent with  
 642 reported changes in Hg emissions from the respective facilities. OSE are found to be the main and  
 643 a major contributor of oxidized Hg concentrations in surface air close to oil sands sources,  
 644 increasing background concentrations over 30% within 100 km and 60% within 50 km from AR6  
 645 in 2012-2013, particularly in the northeast sector of the AOSR. Wildfire emissions played a minor  
 646 role in ambient TOM concentrations in the region, contributing to  $< 1\%$  increases in 2012, 2013  
 647 and 2015, but increased to  $\sim 6\%$  in 2014 as a result of higher wildfire activities. Hg emitted from

648 oil sands operations as oxidized species is deposited efficiently by precipitation and uptake from  
649 terrestrial surfaces in the vicinity of the sources. By comparison, most of the GEM emissions are  
650 transported out of the region except for a small fraction being deposited locally via direct  
651 vegetation uptake and conversion to oxidized species and dry deposition. Oxidized Hg species  
652 emitted from global sources do not reach the AOSR via long-range transport due to their short-  
653 lived nature. As a result, OSE-related Hg deposition in the AOSR consists primarily of TOM,  
654 whereas, long-range transport of GEM accounts for the deposition in the AOSR attributed to  
655 outside sources. Wildfire emissions are mostly assumed to be emitted as GEM as indicated by  
656 observations (Friedli et al. 2001).

657

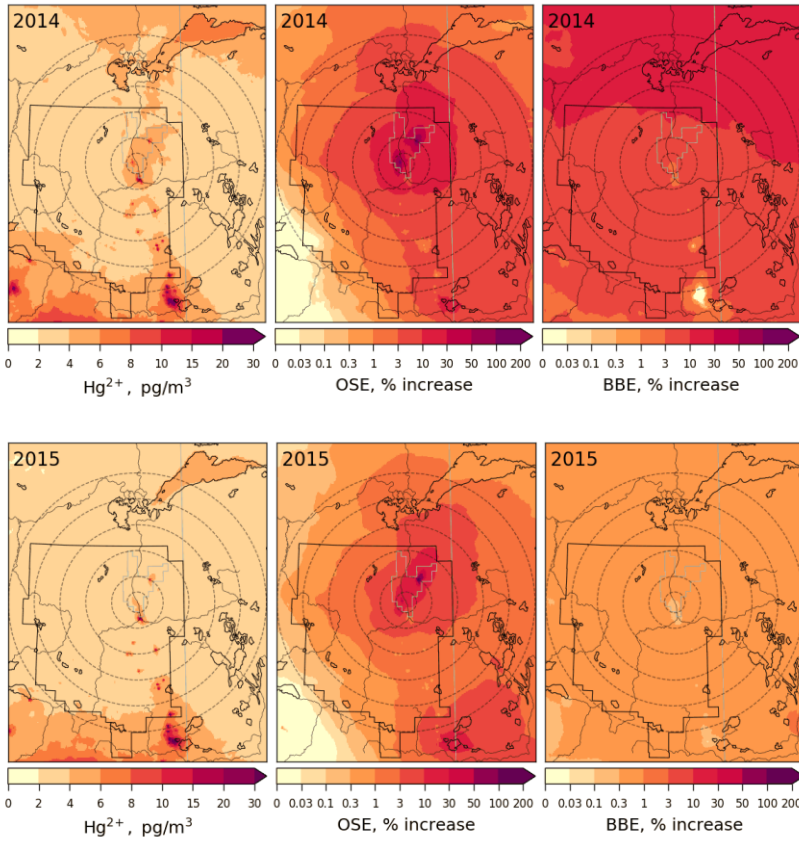


658



659





660

661

662 Figure 13: Annual average surface air concentration of TOM (sum of GOM and PBM, left), and  
 663 concentration enrichments (%) due to Hg emissions from Athabasca oil sands operation (OSE,  
 664 middle) and biomass burning in North America (BBE, right) for the years 2012-2015. AOSR is  
 665 marked as an approximate rectangle and concentric distance circles are at 20, 50, 100, 150, 200  
 666 and 250 km from AR6.

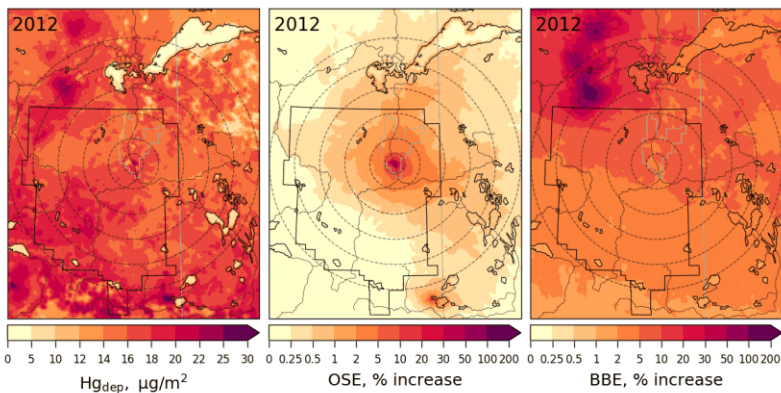
667

668 Figures 14 and 15 provide spatial distributions of modelled annual total mercury deposition (Figure  
 669 14, left panels) and seasonally accumulated Hg loadings in the snow (Figure 15, left panels), and  
 670 their source attributions to OSE (Figure 14, middle panels; Figure 15, right panels) and BBE  
 671 (Figure 14, right panels) in the AOSR in 2012-2015. Mercury deposition fluxes from 7-28  $\mu\text{g m}^{-2}\text{y}^{-1}$   
 672  $(15.6 - 18.3 \mu\text{g m}^{-2}\text{y}^{-1}, \text{averages})$  were modelled in the AOSR in 2012-2015, originating from  
 673 all Hg emission sources - global primary and legacy anthropogenic and geogenic (including oil  
 674 sands and biomass burning) emissions. Since the contribution of global transport of GEM to the  
 675 ambient total Hg concentrations in the AOSR is much larger than the contributions of OSE and  
 676 BBE (Figure 12) and GEM concentrations are typically 2-3 order of magnitude higher than TOM

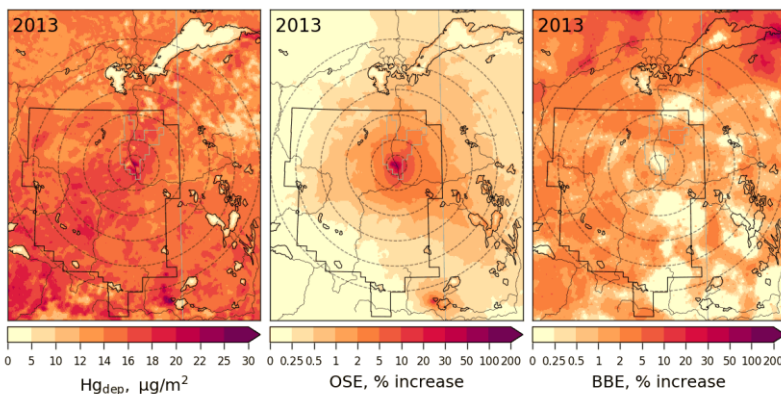
677 concentrations (which have higher contributions from OSE, Figure 13), deposition of imported  
678 GEM makes up a major portion of the annual Hg deposition in the AOSR on a broad spatial scale,  
679 despite its lower Hg deposition efficiencies than TOM (Figure 14). Similar to ambient TOM  
680 concentrations, modelling reveals the impact of OSE to Hg deposition to be greatest in the vicinity  
681 of upgraders, i.e., average increases of 17%, 20%, 8%, and 3% within 20 km of AR6 in 2012,  
682 2013, 2014 and 2015, respectively, and < 1 % beyond 50 km in all years. Model results reveal a  
683 larger impact of OSE on Hg deposition in the regions northeast of oil sands sources, consistent  
684 with observations and prevailing wind direction and speed (Kirk et al. 2014). Average Hg  
685 deposition contributions due to BBE (increases of 1.4-13% ) were higher than OSE contributions  
686 (increases of 0.3-1.3%) across 200 km of oil sands operations in 2012-2015. Wildfires in the  
687 region led to localized increases in Hg deposition of up to 193% and 101% in 2012 and 2014,  
688 especially northwest of the AOSR. Mercury emissions from electricity generation in southern  
689 Alberta accounted for a general decrease in Hg deposition fluxes from south to north around the  
690 AOSR.

691

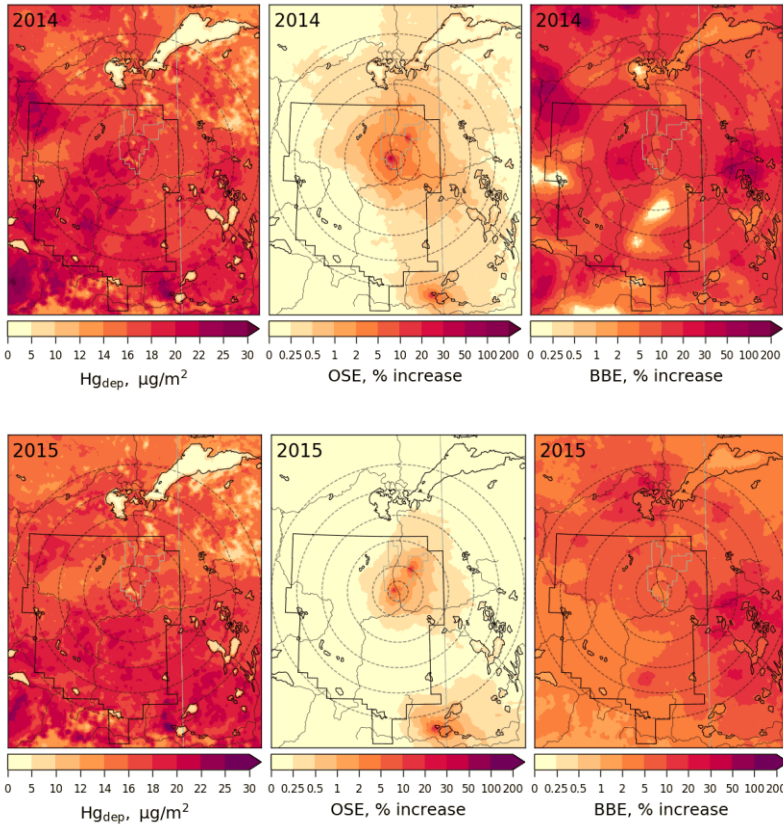
692



693



694



695

696

697 Figure 14: Annual total Hg deposition flux (left) and deposition enrichments (%) due to Hg  
 698 emissions from Athabasca oil sands operations (OSE, middle) and biomass burning in North  
 699 America (BBE, right) in 2012-2015. The AOSR is marked as an approximate rectangle and  
 700 concentric distance circles are at 20, 50, 100, 150, 200 and 250 km from AR6.

701

702 Snowpack Hg accumulations from the start of the snow season to the end of winter (roughly  
 703 coinciding with the maximum snow accumulation period) and their contributions from oil sands  
 704 Hg emissions were estimated for 2012-2015 (Figure 15). Background snow Hg loadings (without  
 705 the impact of OSE, middle panels) were spatially highly variable (up to  $1.4 \mu\text{g m}^{-2}$ ) in the region  
 706 between 2012-2015. The higher snow Hg background levels resulted from both the regional  
 707 transport of Hg from southern Alberta as well as spatial inhomogeneity in the accumulation of  
 708 snow. Closer to OSE sources, total Hg loadings in snow reached up to  $1.0 \mu\text{g m}^{-2}$  (< 20 km from  
 709 AR6) in 2012-2014 (Figure 15). In 2015, emissions from oil sands-related activities were the  
 710 lowest and total Hg loadings corresponded to background emissions. The impact of OSE was  
 711 notably greater to the snowpack Hg loadings, including the spatial extent, than to the annual Hg



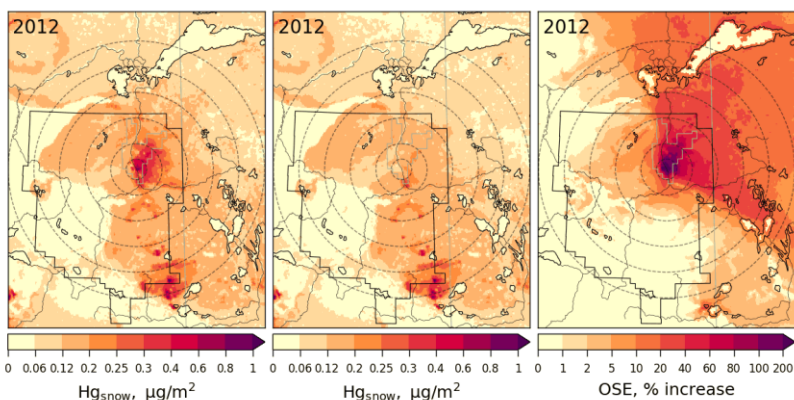
712 deposition (Figure 15, right panels). Average increases of 55%, 43%, 35% and 7% in snow Hg  
713 amounts were simulated within 50 km of AR6 in 2012, 2013, 2014 and 2015, respectively, as a  
714 result of OSE. Regions northeast of the AOSR showed increases of 27-44% in snow Hg levels in  
715 2012 and 2013 and 3-24% in 2014 and 2015 between 50-100 km from AR6. Model results support  
716 the conclusions of previous studies that oil sands Hg emissions have a large impact on snow Hg  
717 loadings near the oil sands emission sources with decreasing contributions away from AR6 (Kelly  
718 et al., 2010; Kirk et al., 2014). The distinctive pattern of higher snow Hg loadings in the northeast  
719 region surrounding the AOSR was also reported (Kirk et al., 2014). Model results reveal high  
720 spatiotemporal variability in background snow Hg loadings; this is related to variability in snowfall  
721 amounts, meteorological conditions affecting melting and snowpack Hg processes including  
722 redox, air-snow exchange and transport to soils.

723  
724 Average annual Hg deposition fluxes in the AOSR were 13.3 (2015) to 18.5 (2013)  $\mu\text{g m}^{-2}\text{y}^{-1}$   
725 within 10 km, 15.0 (2015) to 16.9 (2013)  $\mu\text{g m}^{-2}\text{y}^{-1}$  between 10-20 km, and  $\sim 16 \mu\text{g m}^{-2}\text{y}^{-1}$  50 km  
726 away from the major oil sands emission sources. In the AOSR, winter (and snow cover) can last  
727 up to six months (from November to April) with maximum snow depths in January-February.  
728 Winter (November-April) and summer (June-August) periods contributed to  $\sim 20\%$  and  $50\%$ ,  
729 respectively, of annual Hg deposition in AOSR. In Figure 16, three representative months in the  
730 winter (December to February) and summer (June to August) seasons, each, are chosen to present  
731 the inter-seasonal contrast in OSE impacts on Hg deposition along with the impact on annual  
732 deposition as a function of distance from AR6.

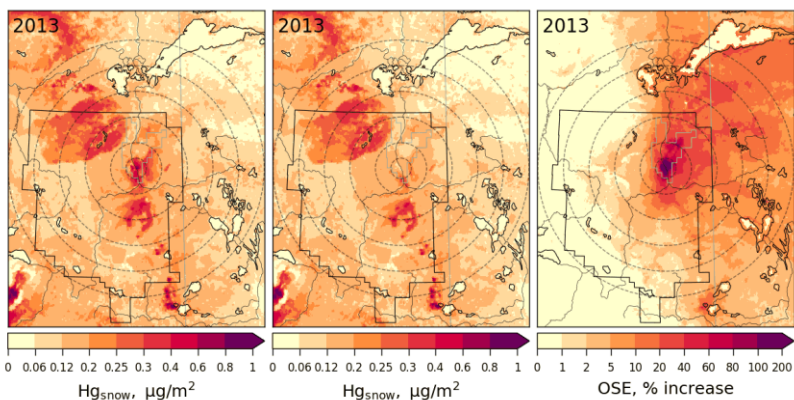
733  
734 Seasonally, OSE accounted for the largest Hg deposition increases in winter months:  $\sim 230\text{-}500\%$   
735 (2013),  $146\text{-}374\%$  (2012),  $94\text{-}104\%$  (2014) and  $40\text{-}43\%$  (2015) within 10 km;  $75\%$  (2013),  $57\%$   
736 (2012),  $25\%$  (2014) and  $5\%$  (2015) at 20 km; and  $24\text{-}33\%$  (2012-2013) and  $6\text{-}12\%$  (2014-2015) at  
737 50 km distance from the major oil sands upgraders. In summertime, lower deposition increases  
738 due to OSE were estimated,  $\sim 13\text{-}56\%$  (2012-2013) and  $3\text{-}7\%$  (2014-2015) within 10 km, and  $<$   
739  $7\%$  (2012-2015) at 20 km from AR6. Annually, OSE accounted for deposition increases of  $\sim 24\text{-}$   
740  $70\%$  (2012-2013),  $14\%$  (2014) and  $< 5\%$  (2015) within 10 km,  $10\%$  (2012-2013) and  $< 5\%$  (2014-  
741 2015) at 20 km, and  $< 4\%$  (2012-2015) at 50 km from the major oil sands emission sources. These  
742 seasonal variations are consistent with inter-seasonal differences in Hg deposition pathways (i.e.

743 the dominant role of GEM uptake by vegetation in summer from global sources, and uptake of  
744 local TOM emissions by snowfall and snowpack as the main pathway in wintertime deposition)  
745 (Graydon et al., 2006; Obrist et al., 2016; Zhang et al. 2009). The influence of OSE to summertime  
746 and annual depositions is also more limited spatially (up to 30 km of OSE) than to wintertime  
747 deposition (up to 100 km of OSE), consistent with observations (Kirk et al, 2014; Gopalapillai et  
748 al., 2019).

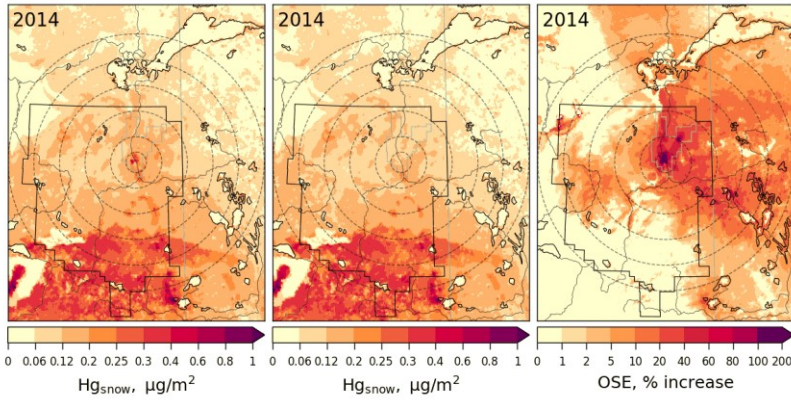
749  
750



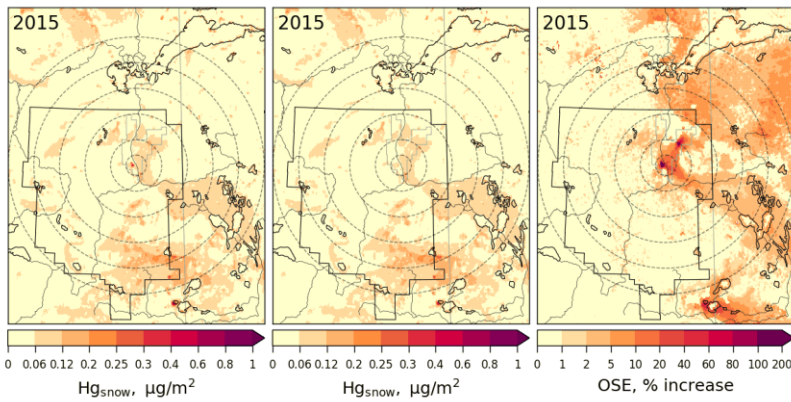
751



752



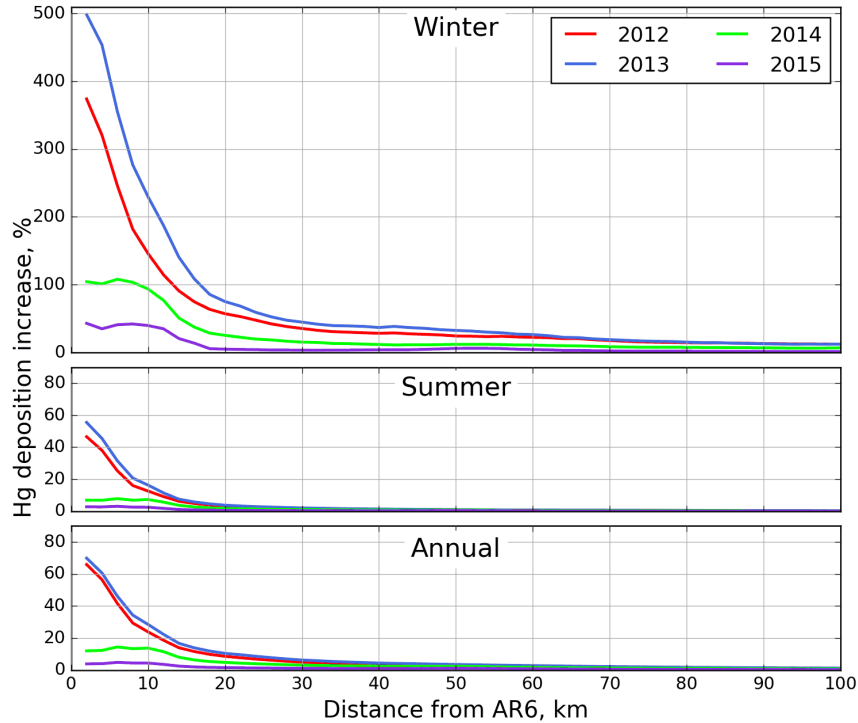
753



754

755 Figure 15: Seasonally accumulated Hg loadings in snow with all Hg emissions (left) and without  
 756 Athabasca oil sands Hg emissions (middle), and enrichments (%) in seasonally accumulated Hg  
 757 loadings in snow due to Athabasca oil sands Hg emissions (OSE, right) in 2012-2015. The AOSR  
 758 is marked as an approximate rectangle and concentric distance circles are at 20, 50, 100, 150, 200  
 759 and 250 km from AR6.

760



761  
 762 Figure 16: Average Hg deposition enrichments (%) due to Athabasca oil sands emissions in winter  
 763 from December to February (top), in summer from June to August (middle), and annually (bottom)  
 764 for 2012 (red), 2013 (blue), 2014 (green) and 2015 (pink) by distance from AR6.

765

766 **Process attribution of interannual variations in mercury deposition**

767 The interannual differences noticed in Figure 16 raises the question of the contributing factors to  
 768 the interannual variability of Hg deposition in different seasons, especially close to the processing  
 769 facilities (i.e., within a 10 and 20 km radius). The relative importance of variations in  
 770 meteorological conditions and changes in OSE and BBE on the temporal changes in Hg deposition  
 771 fluxes from 2012 to 2015 were analyzed. Since meteorological changes are expected to occur  
 772 regardless of changes in emissions, a controlled model simulation was first conducted by applying  
 773 only meteorological changes from 2012 to 2015. Subsequently, two additional model simulations  
 774 were performed by successively adding BBE and OSE changes from 2013-2015. The differences  
 775 in these simulations provided the relative process contributions. It should be noted that, in addition  
 776 to the changes in emissions, the BBE and OSE impacts on Hg deposition also depend on changes  
 777 in meteorological conditions (synoptic as well as local scale), thus the results presented here are  
 778 cumulative contributions of changes in meteorology and emissions. Figure 17 presents process

779 attribution of interannual changes in winter (top), summer (middle) and annual (bottom) Hg  
780 deposition rates from 2012-2015 within 0-10 km (left) and 10-20 km (right) from AR6. The lower  
781 panels illustrate Hg deposition source contributions from global emissions (green; global  
782 anthropogenic (except oil sands), geogenic and re-emission), OSE(red) and BBE(purple), and the  
783 upper panels show process contributions of changes in meteorology (blue), oil sands (red) and  
784 biomass burning (purple) emissions to interannual changes in total Hg deposition.

785  
786 While wintertime Hg deposition fluxes were relatively low ( $2.6\text{-}3.6\ \mu\text{g m}^{-2}$ , November-April;  $0.3$   
787  $\text{--} 0.8\ \mu\text{g m}^{-2}$ , December-February) in the AOSR, oil sands emissions were a major source of Hg  
788 deposition close to the oil sands sources as explained earlier, contributing to 70-80% of deposition  
789 within 10 km of AR6 in high oil sands emission years (2012 and 2013). Wintertime (net) Hg  
790 deposition to northern landscapes is controlled by cryospheric processes, which exhibit strong  
791 interannual variations; therefore, interannual variation in wintertime Hg deposition is strongly  
792 controlled by meteorological conditions including snowfall amounts, wind speed, surface air  
793 temperature, solar insolation, and intra-seasonal melting affecting air-snow-soils exchange  
794 processes of mercury (Faïn et al., 2013). In 2015, a large snowmelt event at the end of February  
795 effectively removed about half of the accumulated mercury in snow resulting in much lower snow  
796 Hg content at the time of sampling (see Figure 9).

797  
798 Surface temperature and intra-seasonal melting have a large impact on how much of the deposited  
799 Hg in the snow is re-emitted back to the atmosphere and how much is adsorbed to surface soils,  
800 altering snow Hg loadings and net wintertime Hg deposition. Since 2013 experienced deeper  
801 snowpack and less inter-seasonal melting, a larger fraction of snowpack Hg was reduced and  
802 revolatilized, leading to a lower net Hg deposition despite slightly higher oil sands Hg emissions  
803 compared to 2012. Conversely, lower snowpack depth and a strong melting event at the end of  
804 February in 2015 allowed a large fraction of snowpack Hg to be transferred and retained in  
805 underlying soils increasing net Hg deposition, particularly the background deposition contribution.

806  
807 Within 10 km of major oil sands sources, wintertime variations in meteorology led to Hg  
808 deposition declines of 17% in 2013 and 2014 and increases of 10% in 2015 along with OSE-led

809 deposition declines of 10% (2013), 35% (2014) and 56% (2015). When combined, the net effect of  
810 these two factors were overall reductions in wintertime Hg deposition fluxes of 27% (2013), 52%  
811 (2014) and 46% (2015), relative to 2012. At a distance of 10-20 km from the oil sands sources,  
812 changes in meteorology led to a 54% increase in wintertime Hg deposition in 2015, but the overall  
813 deposition only increased by 19%, because the decline in oil sands Hg emissions reduced the  
814 deposition by 35%. River discharge rates and Hg concentrations are reported to be highest in the  
815 spring meltwater flood (between 3 ng/L and 16 ng/L, up from typically <2 ng/L at their lowest  
816 annual level) in tributaries of the Athabasca River and pose risk to the downstream environments  
817 (Kelly et al., 2010; Wasiuta et al., 2019). Since the ground is still frozen at the time of spring  
818 freshet, Hg runoff is derived from seasonal snowpack loadings and mobilization of Hg from  
819 surface soils, both of which are contaminated by oil sands emissions in proximity of the sources  
820 and show a sensitivity to changes in Hg emissions from oil sands developments.

821  
822 Compared to winter, AOSR summertime background Hg deposition fluxes were significantly  
823 higher (~6.3-7.5  $\mu\text{g m}^{-2}$ , 2012-2015) and less variable in space and time, and OSE contributions to  
824 total deposition were relatively lower (~0.05-0.5  $\mu\text{g m}^{-2}$  within 10 km and 0.01-0.2  $\mu\text{g m}^{-2}$  from  
825 10-20 km, 2012-2015). In addition, summertime biomass burning emissions contributed to Hg  
826 deposition of 0.1-0.4  $\mu\text{g m}^{-2}$  (2012-2015). Summertime Hg deposition to terrestrial systems is  
827 temporally less variable than wintertime deposition as it is predominantly driven by Hg uptake by  
828 vegetation and soils followed by wet deposition. Changes in oil sands emissions played a more  
829 significant role than the meteorological factors in summertime inter-annual Hg deposition  
830 variations.. Compared to 2012, changes in meteorology, biomass burning and oil sand emissions,  
831 respectively, led to changes in summertime Hg deposition fluxes by -3%, -2%, and +7% in 2013,  
832 +3%, +2% and -15% in 2014, and -1%, +4% and -20% in 2015, resulting in overall changes in Hg  
833 deposition by +2% (2013), -10% (2014) and -17% (2015), within 10 km of major oil sands sources.  
834 Interannual variations in precipitation amounts and its impact on the wet deposition of Hg was the  
835 primary reason for the meteorology-related changes in summertime Hg deposition fluxes.

836  
837 Since summertime deposition contributes to about half of the annual deposition, interannual  
838 changes and their responsible factors in annual Hg deposition fluxes had a similar pattern as  
839 summer, with a relatively larger impact of changes in OSE on Hg deposition fluxes in the

840 immediate vicinity of oil sands sources. Relative to 2012, deposition increases were 6 (2014) and  
 841 1% (2015) due to variations in meteorology and 2% (2014-2015) due to biomass burning, and  
 842 deposition declines were 15 (2014) and 23% (2015) due to reduction in oil sands Hg emissions.  
 843 This results in overall reductions in annual Hg depositions of 7 (2014) and 20% (2015) within 10  
 844 km of AR6. These model results demonstrate that reduction in Hg emissions from oil sands  
 845 processing activities lead to measurable declines in mercury deposition fluxes in AOSR. Further  
 846 away from sources (right panel, Figure 17), the changes in meteorology and oil sands emissions  
 847 resulted in comparable changes in Hg deposition rates (+9 (2014) and +5 % (2015), meteorology;  
 848 -4 (2014) and -9% (2015), OSE) along with 3(2014) and 2(2015)% increases in deposition due to  
 849 BBE, resulting in relatively smaller overall changes (+8% (2014) and -2% (2015)) in Hg deposition  
 850 fluxes. Interestingly, land clearing in the AOSR contributes to reduced background Hg deposition  
 851 fluxes due to the reduction in foliage Hg uptake; average background Hg deposition fluxes were  
 852 about  $1 \mu\text{g m}^{-2}$  lower within 10 km as compared to Hg deposition fluxes 20 km away from the  
 853 major oil sands activities.

854



855

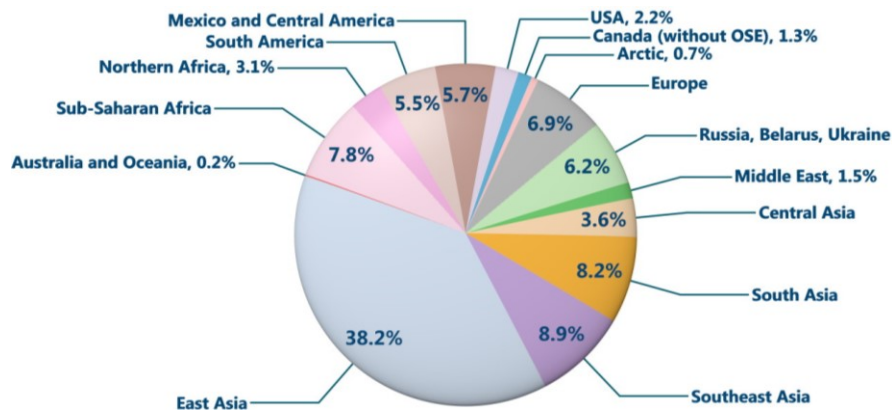
856 Figure 17: (a) December – February, (b) June – August and (c) yearly averaged source  
857 apportionment of total Hg depositions (lower panels) in 2012-2015, and contributions of changes  
858 in meteorology, Athabasca oil sands emissions and biomass burning emissions (only in summer)  
859 (top panels) to the changes in total Hg depositions in 2013-2015 relative to 2012, within 10 km  
860 (left plot) & 10-20 km (right plot) of AR6.

861

### 862 **Source apportionment of the background mercury deposition**

863 As noticed in Figure 14-16, background Hg (long-range transport from global source regions;  
864 excludes impact of oil sands emissions, but includes impact of all other Hg emissions in Canada)  
865 is responsible for the majority of annual Hg deposition in the AOSR (except in winter in the  
866 vicinity of major oil sands Hg emission sources). The average annual background Hg deposition  
867 in the AOSR was  $15.3\text{--}16.7 \mu\text{g m}^{-2}\text{y}^{-1}$  in 2012-2015. This includes ~40% deposition from  
868 contemporary global anthropogenic Hg emissions (excluding Hg emissions from Athabasca oils  
869 sands activities) and ~60% from global geogenic emissions and re-emissions of legacy mercury  
870 deposition (of both anthropogenic and geogenic origin). The model was applied to investigate the  
871 relative proportions of background anthropogenic Hg deposition fluxes contributed from various  
872 worldwide emission source regions, including Canada, in the AOSR (Figure 18). Almost 50% of  
873 the background anthropogenic Hg deposition originated from East and Southeast Asia, a region of  
874 high economic activity and high energy demand, which is sourced for the most part by coal-fired  
875 power plants. The model estimated that foreign anthropogenic sources accounted for over 98% of  
876 the background anthropogenic Hg deposition in the AOSR of which present-day emissions in East  
877 Asia, Southeast Asia, South Asia, Sub-Saharan Africa, Europe and the United States contributed  
878 to approximately 38%, 9%, 8%, 8%, 7%, and 2%, respectively. Emissions from present-day  
879 anthropogenic sources in Canada (excluding oil sands sources in AOSR) contributed to < 2% of  
880 the background anthropogenic Hg deposition nationally including the AOSR. In proximity of oil  
881 sands activities, oil sand Hg emissions are a significant source of Hg deposition as demonstrated  
882 earlier in this study. By comparison, oil sands developments currently have a negligible impact on  
883 Hg deposition on a broader spatial scale in Canada. These results highlight the need for worldwide  
884 mitigation efforts, in addition to the local efforts, to reduce the risks of mercury contamination in  
885 the AOSR.





886  
 887 Figure 18: Deposition contributions from global anthropogenic source regions (excluding  
 888 Athabasca oil sands Hg emissions) to the average contemporary anthropogenic Hg deposition  
 889 portion (40% of total deposition) of the total deposition in Athabasca Oil Sands Region in 2015.  
 890

891 **Conclusions**

892 An assessment of mercury levels in air and deposition in the Athabasca oil sands region (AOSR)  
 893 in Northern Alberta, Canada, was conducted to investigate the contribution of Hg emitted from oil  
 894 sands activities on the surrounding landscape using a 3D process-based Hg model in 2012-2015.  
 895 The model-simulated Hg burden in the region was first evaluated with multi-year observations of  
 896 air concentrations of Hg and seasonally accumulated Hg in snow. Model-measurement agreement  
 897 of Hg surface air concentrations and snow loadings in AOSR were within the measurement and  
 898 modeling uncertainties and implies that NPRI reported emissions of Hg from oil sands operations  
 899 (i.e., 59, 69, 44 and 25 kg in 2012, 2013, 2014 and 2015, respectively) are consistent with Hg  
 900 burden in the region. Air concentrations of Hg(0) in the AOSR (1.4 ng m<sup>-3</sup>) were at a similar level  
 901 as found in Northern Alberta, and were within the range of concentrations in Canada (1.2-1.6 ng  
 902 m<sup>-3</sup>). Background Hg(0) concentrations in Canada are dominated by long-range transport, with a  
 903 slightly larger impact in the west, and, thus, contribution of oil sands activities to Hg(0)  
 904 concentrations in AOSR was minimal (< 0.1%, average enrichment). During the summer season,  
 905 Hg emissions originating from regional wildfires were found to be an episodically important  
 906 source of atmospheric Hg(0), with daily averaged concentrations peaking to 2.5 ng m<sup>-3</sup> (Parsons  
 907 et al. 2013; Fraser et al., 2018). Average total oxidized Hg concentrations (gaseous plus  
 908 particulate) in the air were elevated above background by 55% and 65% in 2012 and 2013,

909 respectively, and over 10% in 2015 within 50 km of upgrading facilities (particularly in the  
910 northeast sector) in the AOSR as a result of oil sands emissions.

911  
912 The level and spatial extent of the impact of oil sands emissions to winter, summer and annual Hg  
913 deposition fluxes were examined in high (2012-2013) and low (2014-2015) oil sands Hg emission  
914 years. In 2012-2015, annual average total Hg deposition fluxes of 15.6-18.3  $\mu\text{g m}^{-2}\text{y}^{-1}$ ) were  
915 simulated in AOSR with deposition in winter (November-April) and summer (June-August)  
916 contributing to 20% and 50%, respectively. The emission sources of Hg deposition in the AOSR  
917 are global anthropogenic (including Canadian emissions), natural and reemissions of legacy Hg  
918 deposition (including biomass burning emissions). Similar to other regions in Canada, on a broader  
919 scale, Hg deposition in the AOSR is dominated by mercury transported from global sources, with  
920 a small (and highly spatiotemporal variable) impact from regional biomass burning events. In  
921 proximity to oil sands sources, however, total Hg deposition in wintertime was largely driven by  
922 oils sands emissions. Deposition increases of up to 146-500% occurred within 10 km of oil sands  
923 sources in the high emission years 2012 and 2013; summertime and annual Hg deposition increases  
924 due to oil sands emissions were 13-56% and 24-70%, respectively, within 10 km of sources for  
925 the same years. In lower oil sands emission years (2014 and 2015), Hg deposition increases due to  
926 oil sands activities declined to 40-104% in winter and 5-14% annually within 10 km of oil sands  
927 sources. At 20 km from the oil sands operations, oil sands-related Hg deposition enhancements  
928 were not as large, with increases of 57-75% in winter, and 10% annually in 2012 and 2013. The  
929 spatial extent of the OSE influence on Hg deposition was also greater in winter relative to summer  
930 (~100 km vs 30 km from major Hg emitting facilities).

931  
932 Finally, factors contributing to the inter-annual variations (i.e., changes in meteorological  
933 conditions, oil sands emissions and wildfire emissions) in seasonal and annual Hg deposition  
934 fluxes and relative source attributions in AOSR were examined from 2012 to 2015. Wintertime  
935 (net) Hg deposition to northern landscapes is controlled by Hg deposition to snowpacks by direct  
936 uptake and via snowfall and post-depositional processes, which exhibit strong inter-annual  
937 variations. Relative to 2012, while changes in meteorological conditions led to a reduction in  
938 wintertime Hg net deposition fluxes by ~ 17% in 2013-2014, and an increase by 10% in 2015  
939 within 10 km of oil sands sources, changes in oil sands emissions led to deposition reductions of

940 10%, 35% and 56% in 2013, 2014 and 2015, respectively, resulting in an overall reduction in  
941 wintertime Hg depositions of 27%, 52% and 46% in 2013, 2014 and 2015, respectively.  
942 Gopalapillai et al. (2019) reported temporal decline in snowpack total Hg loadings near-field, from  
943 an average load of 510 to 175 ng/m<sup>2</sup> from 2008 to 2016. At a distance of 10-20 km from the oil  
944 sands sources, while changes in meteorology led to a 54% increase in wintertime deposition in  
945 2015 relative to 2012, the decline in oil sands emissions led to a reduction in the deposition by  
946 35%, resulting in an overall increase in Hg deposition of 19%. Summertime Hg deposition to  
947 terrestrial systems is temporally less variable than wintertime deposition as it is predominantly  
948 driven by Hg uptake by vegetation and soils, and by wet deposition; thus, changes in oil sands  
949 emissions played a more significant role in summertime inter-annual variations in Hg deposition  
950 than the meteorological factors. Compared to 2012, changes in meteorology, biomass burning and  
951 oil sand emissions led to changes in summertime deposition by -3%, -2%, and +7% in 2013, +3%,  
952 +2% and -15% in 2014, and -1%, +4% and -20% in 2015, resulting in overall changes in Hg  
953 deposition by +2%, -10% and -17% in 2013, 2014 and 2015, respectively, within 10 km of major  
954 oil sands sources. On an annual basis, in 2014 and 2015, variations in meteorology and biomass  
955 burning emissions led to deposition increases of 1-6% and 2%, respectively, and reduction in oil  
956 sands Hg emissions led to declines between 15-22%, resulting in an overall reduction in annual  
957 Hg deposition of 7-20% within 10 km of AR6. In 2015, at 10-20 km away from sources, Hg  
958 deposition increase due to changes in meteorology plus biomass burning was approximately equal  
959 to deposition decline due to changes in oil sands emissions, resulting in smaller (<8%) changes in  
960 Hg deposition fluxes.

961  
962 Oil sands Hg emissions are found to be important sources of Hg contamination to the local  
963 landscape in proximity of the processing activities, particularly in wintertime. Although Hg  
964 deposition is higher in summertime (mainly driven by long-range transport), oil sands Hg  
965 emissions contribute to a notably higher proportion of deposition in wintertime in the AOSR. Thus,  
966 the impact of oil sands emissions is more easily detected in snow Hg observations (Kirk et al.,  
967 2014). Wintertime Hg deposition rates are also more influenced by interannual changes in  
968 meteorological conditions compared to summer. Regarding the environmental importance of  
969 seasonal Hg deposition, it is likely that a major portion of summertime deposition remains bound  
970 to vegetation and subsequently transferred to soils, where it can be partially sequestered and partly

971 reemitted back to air or mobilized in aquatic systems on long timescales of decades to centuries  
972 (Zhou et al. 2021). In contrast, wintertime deposition (and partially summertime wet deposition)  
973 can be transferred to the local aquatic system via runoff more readily (i.e, on an annual time scale).  
974 Model findings reveal that year-to-year changes in meteorological conditions not only significantly  
975 influence the rate of Hg deposition but, additionally, can either exacerbate or diminish the impact  
976 of changes in oil sands emissions on Hg deposition, particularly in winter. Thus, meteorological  
977 changes can confound the interpretation of trends in short-term monitoring data. In addition,  
978 meteorological changes related to climate change can influence the deposition trends. Accurate  
979 reporting of point and area Hg emissions related to oil sands activities, long-term monitoring of  
980 Hg in air and terrestrial ecosystems, and the application of process-based Hg models are crucial to  
981 understanding systematic changes in Hg levels and their causes in the AOSR.

982

### 983 **Acknowledgements**

984 We thank our ECCC colleagues Paul Makar, Sandro Leonardelli and Stewart Cober and in the  
985 Pollutant Inventory and Reporting Division for their insightful comments and careful internal  
986 review of the manuscript. This project was supported by the Joint Oil Sands Monitoring (JOSM)  
987 program of ECCC.

988

989

### 990 **References**

991 Alexander, A. C. and Chambers, P. A.: Assessment of seven Canadian rivers in relation to stages  
992 in oil sands industrial development, 1972–2010, *Environmental Reviews* 24, 484–494,  
993 <https://doi.org/10.1139/er-2016-0033>, 2016.

994 AMAP and UNEP: Technical Background Report for the Global Mercury Assessment 2013.  
995 Chapter 3. Atmospheric Pathways, Transport and Fate., 263, 2013.

996 Angot, H., Dastoor, A., De Simone, F., Gårdfeldt, K., Gencarelli, C. N., Hedgecock, I. M.,  
997 Langer, S., Magand, O., Mastromonaco, M. N., Nordstrøm, C., Pfaffhuber, K. A., Pirrone,  
998 N., Ryjkov, A., Selin, N. E., Skov, H., Song, S., Sprovieri, F., Steffen, A., Toyota, K.,  
999 Travnikov, O., Yang, X., and Dommergue, A.: Chemical cycling and deposition of  
1000 atmospheric mercury in polar regions: review of recent measurements and comparison with

1001 models, *Atmospheric Chemistry and Physics* 16, 10735–10763,  
1002 <https://doi.org/10.5194/acp-16-10735-2016>, 2016.

1003 APEI: Government of Canada, Air Pollutant Emissions Inventory,  
1004 [https://www.canada.ca/en/environment-climate-change/services/pollutants/air-emissions-](https://www.canada.ca/en/environment-climate-change/services/pollutants/air-emissions-inventory-overview.html)  
1005 [inventory-overview.html](https://www.canada.ca/en/environment-climate-change/services/pollutants/air-emissions-inventory-overview.html), accessed 25 Jul 2019

1006 Bieser, J., Slemr, F., Ambrose, J., Brenninkmeijer, C., Brooks, S., Dastoor, A., DeSimone, F.,  
1007 Ebinghaus, R., Gencarelli, C. N., Geyer, B., Gratz, L. E., Hedgecock, I. M., Jaffe, D.,  
1008 Kelley, P., Lin, C.-J., Jaegle, L., Matthias, V., Ryjkov, A., Selin, N. E., Song, S.,  
1009 Travnikov, O., Weigelt, A., Luke, W., Ren, X., Zahn, A., Yang, X., Zhu, Y., and Pirrone,  
1010 N.: Multi-model study of mercury dispersion in the atmosphere: vertical and  
1011 interhemispheric distribution of mercury species, *Atmospheric Chemistry and Physics* 17,  
1012 6925–6955, <https://doi.org/10.5194/acp-17-6925-2017>, 2017.

1013 Bloom, N. S. and Crecelius, E. A.: Determination of mercury in seawater at sub-nanogram per  
1014 liter levels, *Marine chemistry* 14, 49–59, [https://doi.org/10.1016/0304-4203\(83\)90069-5](https://doi.org/10.1016/0304-4203(83)90069-5),  
1015 1983.

1016 CMSA: Canadian Mercury Science Assessment 2016, *Clean Air Regulatory Agenda*, 437–556,  
1017 2016.

1018 Cooke, C. A., Kirk, J. L., Muir, D. C. G., Wiklund, J. A., Wang, X., Gleason, A., and Evans, M.  
1019 S.: Spatial and temporal patterns in trace element deposition to lakes in the Athabasca oil  
1020 sands region (Alberta, Canada), *Environmental Research Letters* 12,  
1021 <https://doi.org/10.1088/1748-9326/aa9505>, 2017.

1022 Dastoor, A. P., Davignon, D., Theys, N., Van Roozendaal, M., Steffen, A., and Ariya, P. A.:  
1023 Modeling dynamic exchange of gaseous elemental mercury at polar sunrise, *Environmental*  
1024 *Science & Technology* 42, 5183–5188, 2008.

1025 Dastoor, A. P. and Durnford, D. A.: Arctic Ocean: Is it a sink or a source of atmospheric  
1026 mercury?, *Environmental Science & Technology* 48, 1707–1717,  
1027 <https://doi.org/10.1021/es404473e>, 2014.

1028 De Simone, F., Cinnirella, S., Gencarelli, C. N., Yang, X., Hedgecock, I. M., and Pirrone, N.:  
1029 Model study of global mercury deposition from biomass burning, *Environmental science &*  
1030 *technology* 49, 6712–6721, 2015.

1031 Durnford, D., Dastoor, A., Figueras-Nieto, D., and Ryjkov, A.: Long range transport of mercury  
1032 to the Arctic and across Canada, *Atmospheric Chemistry and Physics* 10, 6063–6086,  
1033 <https://doi.org/10.5194/acp-10-6063-2010>, 2010.

1034 Durnford, D., Dastoor, A., Ryzhkov, A., Poissant, L., Pilote, M., and Figueras-Nieto, D.: How  
1035 relevant is the deposition of mercury onto snowpacks?—Part 2: A modeling study,  
1036 *Atmospheric Chemistry and Physics* 12, 9251–9274, 2012.

1037 Eckley, C. S., Parsons, M. T., Mintz, R., Lapalme, M., Mazur, M., Tordon, R., Elleman, R.,  
1038 Graydon, J. A., Blanchard, P., and St Louis, V.: Impact of closing Canada’s largest point-  
1039 source of mercury emissions on local atmospheric mercury concentrations., *Environ Sci*  
1040 *Technol* 47, 10339–10348, <https://doi.org/10.1021/es401352n>, 2013.

1041 Emmerton, C. A., Cooke, C. A., Wentworth, G. R., Graydon, J. A., Ryjkov, A., and Dastoor, A.:  
1042 Total Mercury and Methylmercury in Lake Water of Canada’s Oil Sands Region., *Environ*  
1043 *Sci Technol* 52, 10946–10955, <https://doi.org/10.1021/acs.est.8b01680>, 2018.

1044 EPA: United States Government: EPA Air Emissions Inventories, [https://www.epa.gov/air-](https://www.epa.gov/air-emissions-inventories)  
1045 [emissions-inventories](https://www.epa.gov/air-emissions-inventories); accessed 25 Jul 2019

1046 EPA: Method 1669: Sampling ambient water for trace metals at EPA water quality criteria  
1047 levels, 1996.

1048 Faïn, X., Helmig, D., Hueber, J., Obrist, D., and Williams, M. W.: Mercury dynamics in the  
1049 Rocky Mountain, Colorado, snowpack, *Biogeosciences* 10, 3793–3807, 2013.

1050 Fraser, A., Dastoor, A., and Ryjkov, A.: How important is biomass burning in Canada to  
1051 mercury contamination, *Atmospheric Chemistry and Physics* 18, 7263,  
1052 <https://doi.org/10.5194/acp-18-7263-2018>, 2018.

1053 Friedli, H. R., Radke, L. F., and Lu, J. Y.: Mercury in smoke from biomass fires, *Geophysical*  
1054 *Research Letters* 28, 3223–3226, 2001.

1055 GoC: Government of Canada, Historical Climate Data, <https://climate.weather.gc.ca>, accessed 19  
1056 Feb 2019

1057 Gopalapillai, Y., Kirk, J. L., Landis, M. S., Muir, D. C. G., Cooke, C. A., Gleason, A., Ho, A.,  
1058 Kelly, E., Schindler, D., Wang, X., and Lawson, G.: Source Analysis of Pollutant Elements  
1059 in Winter Air Deposition in the Athabasca Oil Sands Region: A Temporal and Spatial  
1060 Study, *ACS Earth and Space Chemistry* 3, 1656–1668,  
1061 <https://doi.org/10.1021/acsearthspacechem.9b00150>, 2019.

1062 Graydon, J. A., St. Louis, V. L., Lindberg, S. E., Hintelmann, H., and Krabbenhoft, D. P.:  
1063 Investigation of Mercury Exchange between Forest Canopy Vegetation and the  
1064 Atmosphere Using a New Dynamic Chamber, *Environmental Science & Technology*  
1065 40, 4680–4688, <https://doi.org/10.1021/es0604616>, 2006.

1066 Gustin, M. S., Huang, J., Miller, M. B., Peterson, C., Jaffe, D. A., Ambrose, J., Finley, B. D.,  
1067 Lyman, S. N., Call, K., Talbot, R., Feddersen, D., Mao, H., and Lindberg, S. E.: Do We  
1068 Understand What the Mercury Speciation Instruments Are Actually Measuring? Results of  
1069 RAMIX., *Environmental Science & Technology* <https://doi.org/10.1021/es3039104>,  
1070 2013.

1071 Gustin, M. S., Amos, H. M., Huang, J., Miller, M. B., and Heidecorn, K.: Measuring and  
1072 modeling mercury in the atmosphere: a critical review, *Atmos. Chem. Phys.*, 15, 5697–  
1073 5713, <https://doi.org/10.5194/acp-15-5697-2015>, 2015.

1074 Jia, L.: Oil Sands Bitumen Emulsion Upgrading by Using In Situ Hydrogen Generated through  
1075 the Water Gas Shift Reaction, 2014.

1076 Kelly, E. N., Schindler, D. W., Hodson, P. V., Short, J. W., Radmanovich, R., and Nielsen, C.  
1077 C.: Oil sands development contributes elements toxic at low concentrations to the  
1078 Athabasca River and its tributaries, *Proceedings of the National Academy of Sciences* 107,  
1079 16178–16183, <https://doi.org/10.1073/pnas.1008754107>, 2010.

1080 Kirk, J. L., Muir, D. C. G., Gleason, A., Wang, X., Lawson, G., Frank, R. A., Lehnher, I., and  
1081 Wrona, F.: Atmospheric deposition of mercury and methylmercury to landscapes and  
1082 waterbodies of the Athabasca oil sands region, *Environmental science & technology* 48,  
1083 7374–7383, 2014.

1084 Kos, G., Ryzhkov, A., Dastoor, A., Narayan, J., Steffen, A., Ariya, P. A., and Zhang, L.:  
1085 Evaluation of discrepancy between measured and modelled oxidized mercury species,  
1086 *Atmospheric Chemistry and Physics* 13, 4839–4863, [https://doi.org/10.5194/acp-13-4839-](https://doi.org/10.5194/acp-13-4839-2013)  
1087 2013, 2013.

1088 Larter, S. R. and Head, I. M.: Oil sands and heavy oil: origin and exploitation, *Elements* 10, 277–  
1089 283, 2014.

1090 Lynam, M., Dvonch, J. T., Barres, J., and Percy, K.: Atmospheric wet deposition of mercury to  
1091 the Athabasca oil sands region, Alberta, Canada, *Air Quality, Atmosphere & Health* 11,  
1092 83–93, 2018.

1093 Ma, J., Hintelmann, H., Kirk, J., and Muir, D.: Mercury concentrations and mercury isotope  
1094 composition in lake sediment cores from the vicinity of a metal smelting facility in Flin  
1095 Flon, Manitoba, Chemical Geology <https://doi.org/10.1016/j.chemgeo.2012.10.037>, 2012.

1096 Makar, P., Akingunola, A., Pabla, B., Stroud, C., Chen, J., Cheung, P., Moran, M., Gong, W.,  
1097 Zheng, Q., and Li, S. M.: Experimental Forecasting Using the High-Resolution Research  
1098 Configuration of GEM-MACH, International Technical Meeting on Air Pollution  
1099 Modelling and its Application, 225–230, 2018.

1100 Muir, D.C.G., Wang, X., Yang, F., Nguyen, N., Jackson, T.A., Evans, M.S., Douglas, M., Kock, G.,  
1101 Lamoureux, S., Pienitz, R., Smol, J.P., Vincent, W.F., Dastoor, A. (2009). ‘Spatial trends and historical  
1102 deposition of mercury in eastern and northern Canada inferred from lake sediment cores.’ Environment  
1103 Science & Technology, 43, 4802 – 4809.

1104

1105 NPRI: Government of Canada, Access the reporting guide for the National Pollutant Release  
1106 Inventory, [https://www.canada.ca/en/environment-climate-change/services/national-](https://www.canada.ca/en/environment-climate-change/services/national-pollutant-release-inventory/report/access-reporting-guide.html)  
1107 [pollutant-release-inventory/report/access-reporting-guide.html](https://www.canada.ca/en/environment-climate-change/services/national-pollutant-release-inventory/report/access-reporting-guide.html), accessed 25 Jul 2019

1108 NPRI: Government of Canada, National Pollutant Release Inventory, [https://www.ec.gc.ca/inrp-](https://www.ec.gc.ca/inrp-npri/)  
1109 [npri/](https://www.ec.gc.ca/inrp-npri/), accessed 25 Jul 2019

1110 Obrist, D., Johnson, D. W., and Edmonds, R. L.: Effects of vegetation type on mercury  
1111 concentrations and pools in two adjacent coniferous and deciduous forests, Journal of Plant  
1112 Nutrition and Soil Science 175, 68–77, <https://doi.org/10.1002/jpln.201000415>, 2012.

1113 Obrist, D. *et al.* A synthesis of terrestrial mercury in the western United States: Spatial  
1114 distribution defined by land cover and plant productivity. *Science of the Total Environment*  
1115 568, 522-535, doi:10.1016/j.scitotenv.2015.11.104 (2016).

1116 Parsons, M., McLennan, D., Lapalme, M., Mooney, C., Watt, C., and Mintz, R.: Total gaseous  
1117 mercury concentration measurements at Fort McMurray, Alberta, Canada, Atmosphere 4,  
1118 472–493, <https://doi.org/10.3390/atmos4040472>, 2013.

1119 Steffen, A. and Schroeder, W. H.: Standard Operating Procedures Manual Procedure for Total  
1120 Gaseous Mercury Measurements-Canadian Atmospheric Mercury Measurement Network  
1121 (CAMNet), Meteorological Service of Canada 4905, 1999.

1122 Travnikov, O., Angot, H., Artaxo, P., Bencardino, M., Bieser, J., D’Amore, F.,  
1123 Dastoor, A., De Simone, F., Diéguez, M. D. C., Dommergue, A., Ebinghaus, R., Feng, X.



1124 B., Gencarelli, C. N., Hedgecock, I. M., Magand, O., Martin, L., Matthias, V., Mashyanov,  
1125 N., Pirrone, N., Ramachandran, R., Read, K. A., Ryjkov, A., Selin, N. E., Sena, F., Song,  
1126 S., Sprovieri, F., Wip, D., Wängberg, I., and Yang, X.: Multi-model study of mercury  
1127 dispersion in the atmosphere: atmospheric processes and model evaluation, *Atmospheric*  
1128 *Chemistry and Physics* 17, 5271–5295, <https://doi.org/10.5194/acp-17-5271-2017>, 2017.  
1129 UN: Minamata Convention on Mercury, 72, 2017, <http://www.mercuryconvention.org>.  
1130 UNEP: The Global Atmospheric Mercury Assessment: Sources, Emissions and Transport, 2008.  
1131 UNEP: Global Mercury Assessment 2013, Sources, Emissions, Releases and Environmental  
1132 Transport, 2013.  
1133 UNEP: Global Mercury Assessment 2018, 2018.  
1134 Wasiuta, V., Kirk, J. L., Chambers, P. A., Alexander, A. C., Wyatt, F. R., Rooney, R. C., and  
1135 Cooke, C. A.: Accumulating Mercury and Methylmercury Burdens in Watersheds  
1136 Impacted by Oil Sands Pollution., *Environ Sci Technol* 53, 12856–12864,  
1137 <https://doi.org/10.1021/acs.est.9b02373>, 2019.  
1138 Whaley, C. H., Galarneau, E., Makar, P. A., Akingunola, A., Gong, W., Gravel, S., Moran, M.  
1139 D., Stroud, C., Zhang, J., and Zheng, Q.: GEM-MACH-PAH (rev2488): a new high-  
1140 resolution chemical transport model for North American polycyclic aromatic hydrocarbons  
1141 and benzene, *Geoscientific Model Development* 11, 2609–2632,  
1142 <https://doi.org/10.5194/gmd-11-2609-2018>, 2018.  
1143 Wiedinmyer, C., Akagi, S. K., Yokelson, R. J., Emmons, L. K., Al-Saadi, J. A., Orlando, J. J.,  
1144 and Soja, A. J.: The Fire INventory from NCAR (FINN): A high resolution global model to  
1145 estimate the emissions from open burning, *Geoscientific Model Development* 4, 625, 2011.  
1146 Wiedinmyer, C. and Friedli, H.: Mercury emission estimates from fires: An initial inventory for  
1147 the United States, *Environmental science & technology* 41, 8092–8098,  
1148 <https://doi.org/10.1021/es071289o>, 2007.  
1149 Willis, C. E., Kirk, J. L., St Louis, V. L., Lehnerr, I., Ariya, P. A., and Rangel-Alvarado, R. B.:  
1150 Sources of Methylmercury to Snowpacks of the Alberta Oil Sands Region: A Study of In  
1151 Situ Methylation and Particulates., *Environ Sci Technol* 52, 531–540,  
1152 <https://doi.org/10.1021/acs.est.7b04096>, 2018.  
1153 Willis, C. E., St Louis, V. L., Kirk, J. L., St Pierre, K. A., and Dodge, C.: Tailings ponds of the  
1154 Athabasca Oil Sands Region, Alberta, Canada, are likely not significant sources of total

1155 mercury and methylmercury to nearby ground and surface waters., *Sci Total Environ* 647,  
1156 1604–1610, <https://doi.org/10.1016/j.scitotenv.2018.08.083>, 2019.

1157 Wright, L. P., Zhang, L., and Marsik, F. J.: Overview of mercury dry deposition, litterfall, and  
1158 throughfall studies, *Atmospheric Chemistry and Physics* 16, 13399,  
1159 <https://doi.org/10.5194/acp-16-13399-2016>, 2016.

1160 Zhang, L., Wright, L. P. & Blanchard, P. A review of current knowledge concerning dry  
1161 deposition of atmospheric mercury. *Atmospheric Environment* 43, 5853-5864, 2009.

1162 Zhang, J., Moran, M. D., Zheng, Q., Makar, P. A., Baratzadeh, P., Marson, G., Liu, P., and Li,  
1163 S.-M.: Emissions preparation and analysis for multiscale air quality modeling over the  
1164 Athabasca Oil Sands Region of Alberta, Canada, *Atmospheric Chemistry and Physics* 18,  
1165 10459–10481, 2018.

1166 Zhang, L., Wu, Z., Cheng, I., Wright, L. P., Olson, M. L., Gay, D. A., Risch, M. R., Brooks, S.,  
1167 Castro, M. S., Conley, G. D., Edgerton, E. S., Holsen, T. M., Luke, W., Tordon, R., and  
1168 Weiss-Penzias, P.: The estimated six-year mercury dry deposition across North America,  
1169 *Environ. Sci. Technol.*, 50, 12864–12873, <https://doi.org/10.1021/acs.est.6b04276>, 2016.

1170 Zhou, J., Obrist, D., Dastoor, A., Jiskra, M., and Ryjkov, A.: Vegetation uptake of mercury and  
1171 impacts on global cycling, *Nature Reviews Earth & Environment*, 1-16,  
1172 <https://doi.org/10.1038/s43017-021-00146-y>, 2021.

1173